CrossMark

Collapse Vulnerability and Fragility Analysis of Substandard RC Bridges Rehabilitated with Different Repair Jackets Under Post-mainshock Cascading Events

Mostafa Fakharifar[1], Genda Chen[2],*, Ahmad Dalvand[3], and Anoosh Shamsabadi[4]

Abstract: Past earthquakes have signaled the increased collapse vulnerability of mainshock-damaged bridge piers and urgent need of repair interventions prior to subsequent cascading hazard events, such as aftershocks, triggered by the mainshock (MS). The overarching goal of this study is to quantify the collapse vulnerability of mainshock-damaged substandard RC bridge piers rehabilitated with different repair jackets (FRP, conventional thick steel and hybrid jacket) under aftershock (AS) attacks of various intensities. The efficacy of repair jackets on post-MS resilience of repaired bridges is quantified for a prototype two-span single-column bridge bent with lap-splice deficiency at column-footing interface. Extensive number of incremental dynamic time history analyses on numerical finite element bridge models with deteriorating properties under back-to-back MS-AS sequences were utilized to evaluate the efficacy of different repair jackets on the post-repair behavior of RC bridges subjected to AS attacks. Results indicate the dramatic impact of repair jacket application on post-MS resilience of damaged bridge piers—up to 45.5 % increase of structural collapse capacity—subjected to aftershocks of multiple intensities. Besides, the efficacy of repair jackets is found to be proportionate to the intensity of AS attacks. Moreover, the steel jacket exhibited to be the most vulnerable repair intervention compared to CFRP, irrespective of the seismic sequence (severe MS-severe or moderate AS) or earthquake type (near-fault or far-fault).

Keywords: earthquake damage, rapid repair, RC column, performance-based seismic engineering.

1. Introduction

Past earthquakes have demonstrated catastrophic structural failure of mainshock-damaged structures subjected to cascading events, defined as events likely to be triggered by the main earthquake, such as aftershocks, explosions and tsunamis (Li et al. 2014; Ribeiro et al. 2014). This study is focused on multiple earthquakes consisting of the mainshock (MS) and aftershocks. Multiple earthquakes occur after the first ground shaking, where all the accumulated strain in the

fault system is not relieved at the onset of the first rupture of the faulted area. Thus, sequential ruptures take place until the fault system is completely stabilized (Abdelnaby and Elnashai 2014; Li et al. 2014; Di Sarno 2013). The sequential fault ruptures after the first earthquake, causes multiple earthquakes which are often referred to as foreshock (FS), MS and aftershock (AS) events. The March, 2011 Tohuku, Japan subduction earthquake with a moment magnitude (M_w) of 9 was succeeded by hundreds of aftershocks including at least thirty aftershocks greater than M_w 6 (USGS 2012). While the aftershocks are usually smaller in magnitude compared to the MS, however, aftershocks may have higher intensity, with a longer effective duration; different spectral shape, energy content; and specific energy density compared to the MS (Nazari et al. 2013; Li et al. 2014). The large subduction earthquakes, such as the Maule-Chile earthquake (Feb. 2010, M_w 8.8), Sumatra–Andaman earthquake (Dec. 2004, M_w 9.2) and Tokachi-Oki earthquake (Sep. 2003, M_w 8.1), feature very long duration earthquakes consisting of series of foreshocks, mainshock and aftershocks (USGS 2012; Yang 2009). Even for the modern constructions, the shallow crustal earthquakes (including single earthquake event) are only included for the design and the subduction earthquakes are not considered (White and Ventura 2004; Yang 2009).

MS-damaged structures are vulnerable to aftershocks even when only minor damage is present from the MS (Li et al. 2012, 2014; Di Sarno 2013; Abdelnaby and Elnashai 2014).

[1]Department of Civil, Architectural and Environmental Engineering, Missouri University of Science and Technology, Rolla, MO 65409, USA.

[2]Missouri University of Science and Technology, Rolla, MO 65409, USA.

*Corresponding Author; E-mail: gchen@mst.edu

[3]Department of Engineering, Lorestan University, Khorramabad, Iran.

[4]Office of Earthquake Engineering, California Department of Transportation, Sacramento, CA 95816, USA.

The May 12, 2008 Wenchuan earthquake with a M_w of 7.9 was followed by numerous aftershocks, where the August 5, 2008 aftershock (M_w larger than 6) (USGS 2012) contributed to collapse of many of the structures sustaining damage from the MS event, and causing more loss of life (about 90,000 dead or missing) (Li et al. 2012; Yang 2009). While the delay between a MS and the largest AS could range from minutes to months and it is difficult to predict, however magnitudes of AS are relatively easy to predict (Scholz 2002; Li et al. 2012). Bridge columns are one of the most vulnerable structural elements during seismic events (Priestley et al. 1996; Buckle et al. 2006; Fakharifar et al. 2013, 2014a; Lin et al. 2013). Subsequently, rapid repair of the damaged bridge columns, specifically substandard columns (insufficient confinement in the plastic hinge and longitudinal reinforcement lap-spliced at column-footing interface) after the first seismic event is vital for the post-MS integrity and collapse prevention of the bridge under subsequent aftershocks. Different rehabilitation methods for RC bridge columns, utilizing thin steel jackets (typical 0.5–1.2 mm thick) (Ying et al. 2006), carbon fiber reinforced polymer (CFRP) wraps, conventional thick steel jackets (typical 10–50 mm) (Priestley et al. 1996), reinforced concrete jackets, prestressing strands (PS) and shape memory alloy (SMA) wraps have been investigated in different studies (Ying et al. 2006; Priestley et al. 1996; Buckle et al. 2006; Vosooghi and Saiidi 2012; Fakharifar et al. 2014a, c, 2015a; Andrawes et al. 2009). Shear deficient columns are excluded from this study, as the shear deficient columns require rehabilitation prior to any seismic event.

The post-MS load carrying capacity of earthquake damaged structures depends on the extent of damage present (Aschheim and Black 1999; Terzic and Stojadinovic 2013; Priestley et al. 1996; Buckle et al. 2006; Vosooghi and Saiidi 2012; Fakharifar et al. 2014a; He et al. 2013; Grelle and Sneed 2013). While numerous studies have investigated the significance and efficacy of retrofit jackets application on RC bridge columns (Priestley et al. 1996; Buckle et al. 2006; Vosooghi and Saiidi 2012; Fakharifar et al. 2014a; He et al. 2013; ElGawady et al. 2009; Saatcioglu and Yalcin 2003 amongst many others), this study is a preliminary attempt to investigate the efficacy of different repair jackets application on MS-damaged RC bridge piers subjected to AS attacks of multiple intensities. Study by Huang and Andrawes (2014) indicated very promising results that an improvement as high as 117 % in bridge overall performance subjected to real strong mainshock-aftershock sequences can be achieved through applying SMA confinement to piers.

It is an unrealistic assumption that the structure would be repaired to its intact/undamaged state prior to the next seismic event, which is commonly assumed in seismic loss estimation (Nazari et al. 2013). Hence, this study aims at quantifying the impact of repair jackets on the post-MS collapse capacity of repaired bridges with substandard reinforcement detailing under AS attacks. While considering the effects of multiple (successive) earthquakes or sometimes referred to as long-duration earthquakes on the non-linear response of structures has been the topic of numerous research studies (Chang et al. 2012; Di Sarno 2013; Li et al.

2014), however, to the best of the authors' knowledge, there is no comprehensive study on different repair jackets application on MS-damaged RC bridge structures subjected to AS attacks of multiple intensities of different earthquake types. Few studies have attempted to account for the prior damage effect, particularly when the structures are being repaired after the first seismic attack. The first method to include the existing damage condition prior to repair is to modify the material properties of the repaired region—for example reducing the structure's initial stiffness—to account for the effect of previous damage and repair (Aschheim and Black 1999). The second approach to incorporate the degraded strength and stiffness of members due to existing damage is through the use of time-dependent repair elements that can be activated (birth) [or deactivated (death)] within the user-defined time intervals of interest during static and dynamic time-history analysis (Lee et al. 2009, 2011).

Many studies have indicated the seismic vulnerability of MS-damaged bridge columns, if subjected to potential aftershocks, as substantial damage could accumulate during the MS event (Vosooghi and Saiidi 2012; Di Sarno 2013; He et al. 2013; Li et al. 2014). A MS-AS (or often termed FS-AS) sequence is illustrated in Fig. 1a. The Arias intensity (Arias 1970) plot for the MS only and MS-AS sequence are depicted in Fig. 1b, which shows that the energy accumulates over a longer time for the MS-AS sequence (longer duration ground motion) as compared to the MS only (shorter ground motion). The energy flux plot in Fig. 1c, as a measure of seismic energy content, shows the second increase due to AS effect compared to one ground motion. Safety and integrity of a bridge structure subjected to such seismic event heavily depends on the capacity of bridge columns to dissipate the seismic input energy through inelastic hysteretic cycles. Figure 2a illustrates an RC single column bridge bent subjected to a MS-AS sequence. Figure 2b depicts the bridge at incipient collapse after the MS attack and the repair jacket application in the plastic hinge region of the damaged column prior to the AS attack. Figure 2c illustrates the impact of existing damage from the MS event on reducing the lateral load carrying capacity of the damaged structure subjected to AS. It is clear that if repair jackets (e.g. CFRP wraps or steel plate jackets) are implemented, the repaired bridge column could sustain considerably higher drift ratios compared to the unrepaired bridge column. On the contrary, the unrepaired bridge bent experienced rapid strength deterioration with degrading post-peak strength. It could be noticed that there is a direct correlation between damage state from the MS event and the bridge resilience to the AS event, and appropriately designed/implemented repair jackets could enhance the bridge post-repair seismic performance.

2. Research Significance

The overarching goal of this study is to evaluate the damage from MS-AS sequences of multiple intensities on substandard bridge piers (local behavior) and quantify the efficacy of different repair jackets on the post-MS collapse
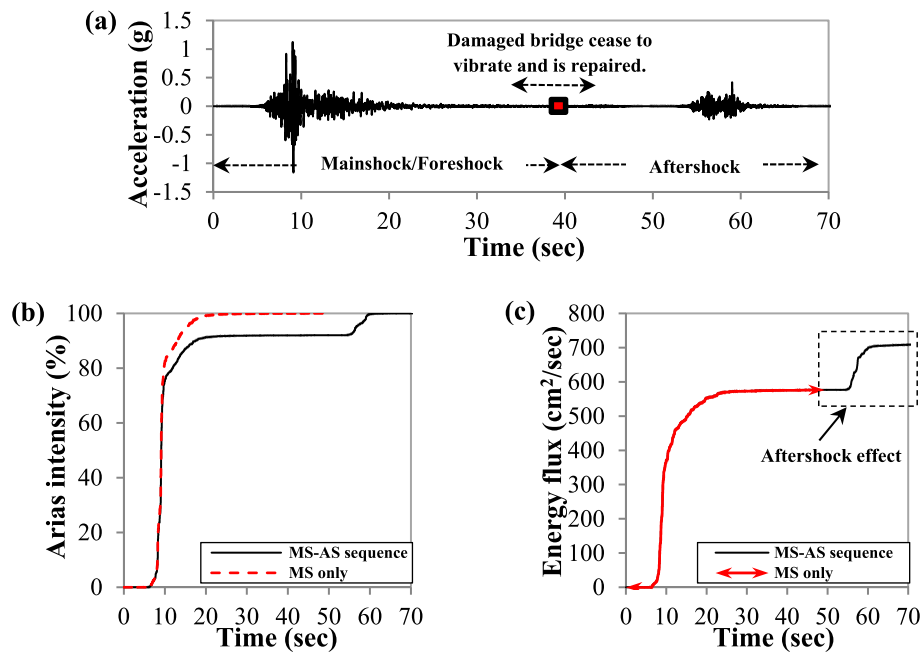
Fig. 1 **a** A typical mainshock-aftershock pair acceleration time-history sequence, **b** arias intensity for mainshock (MS) only and mainshock-aftershock (MS-AS) sequence, and **c** energy flux for MS and MS-AS sequence.

capacity of rehabilitated bridges (system behavior) under aftershocks. To achieve this goal, a two-span, substandard single-column bent RC bridge, typical of older construction practice, is utilized as a reference bridge to illustrate the impact of repair jacket application on damaged bridges subjected to AS attacks. The state of damage and structural collapse capacity under the MS-AS excitations is quantified through incremental dynamic analysis procedure. Different repair jackets, namely CFRP, conventional thick steel, and a proposed hybrid jacket are considered as repair interventions. Different repair jackets were considered to evaluate potential disparities on the post-repair behavior of bridges upon introducing different confining jackets, which results in different levels of confining pressure and confinement type (steel or FRP-based confined models). Results from different seismic sequences of various intensities are presented in detail, and effects of different earthquake types on structural collapse capacity and fragility of the repaired and unrepaired bridge are highlighted.

3. Prototype Highway Bridge Structure

One type of the most common class of highway bridges was selected for this investigation. The bridge was a two-span bridge seated on two abutments and one single column-bent (see Fig. 3). The two spans were 36.5 m long each, with a single cell box girder with a width of 8.22 m. The column longitudinal reinforcement was lap-spliced ($20d_b$, where d_b is the longitudinal reinforcement diameter) at column footing interface. The column is 6.70 tall with a 1.20 diameter. The longitudinal reinforcement of the column cross section consisted of 24 No. 8 ($d_b = 25.4$ mm) lap-spliced reinforcement bars, and the transverse reinforcement

consisted of No. 4 ($d_b = 12$ mm) spiral deformed bars spaced every 102 mm (Fig. 3b). The column is seismically deficient in accordance to modern seismic codes, as the reinforcement is spliced at the potential plastic hinge region. The column was investigated to ensure shear failure is not the governing mode of failure, as shear failure is a catastrophic failure, and retrofitting measures must be implemented prior to any seismic event (e.g. MS). The column aspect ratio is well above 2.5 (i.e., flexural dominant column, exhibiting flexural failure due to formation of a plastic hinge). The material properties constitute the reinforcing steel with a design yield strength of 300 MPa, while the design compressive strength of the concrete was 28 MPa.

4. Confining Repair Jackets for Bridge Pier Rehabilitation

4.1 Hybrid Repair Jacket

Recently, the authors have proposed and experimentally validated a hybrid jacket for the repair of severely damaged RC bridge piers (Fakharifar et al. 2015b). The hybrid jacket comprised of passive and active confining pressure. The hybrid jacket application on the plastic hinge region of a severely damaged RC bridge column is illustrated in Fig. 4. The hybrid jacket is composed of a thin cold-formed steel sheet wrapped around the column with prestressing strands placed over the column. While the prestressing strands can prevent buckling of the confining steel sheet, the thin steel sheet can in turn prevent the prestressing strands from penetrating into cracked cover concrete (i.e., preventing loss of confining pressure in the active strands). The thin cold formed sheet metal is directly wrapped and welded around
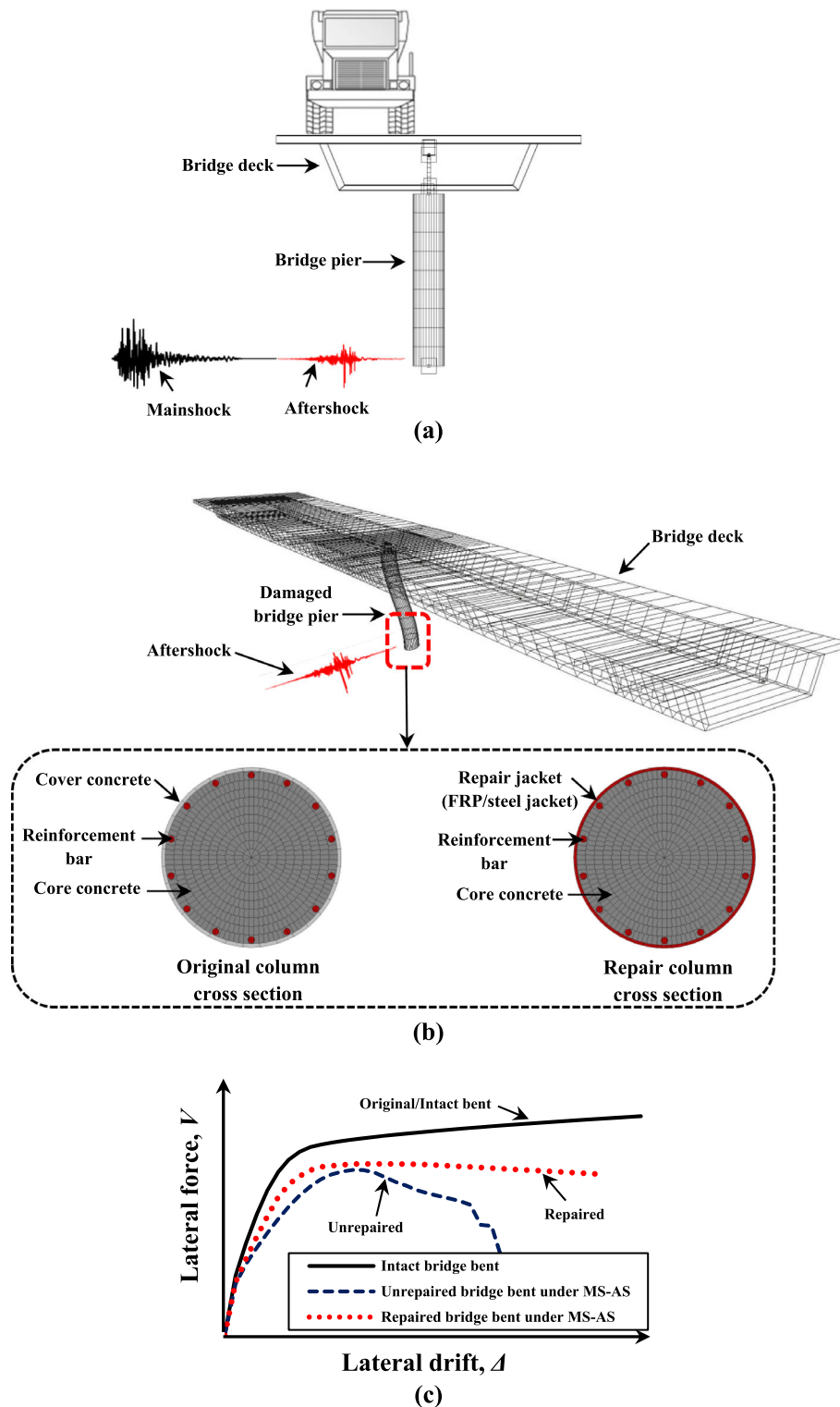
Fig. 2 Repair jacket application on mainshock-damaged single column RC bridge pier, **a** bridge pier subjected to mainshock-aftershock sequence; **b** bridge pier at incipient collapse after the mainshock with/without repair jacket in the plastic hinge region, and **c** representative lateral force–displacement relationship of a bridge bent in the original, unrepaired and repaired condition.

the existing column. The repair is completed by placing and prestressing the strands around the column. The hybrid jacket exhibits advantageous features over traditional repair jackets such as feasibility of rapid application after a MS event (no heavy equipment required); no additional seismic weight introduced due to small thickness of sheet metal and negligible weight of cables (similar to FRP jackets); and no

requirement for column surface preparation and adhesive material application (required for FRP jackets). The most prominent structural feature of the hybrid jacket is resisting the shear crack opening in both the vertical and horizontal directions (see Fig. 5), while the prestressing strands (similarly any unidirectional jacket such as FRP or SMA wires) can resist the shear crack opening in the transverse direction
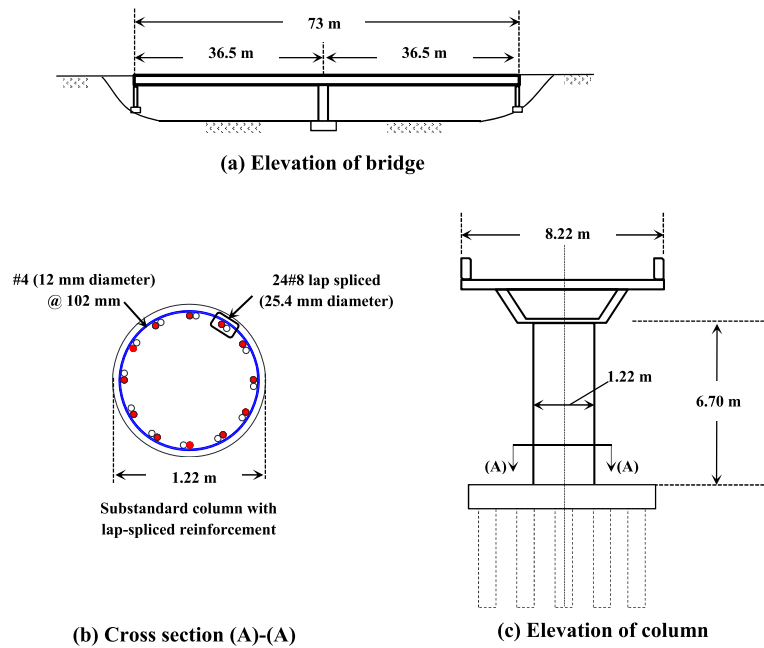
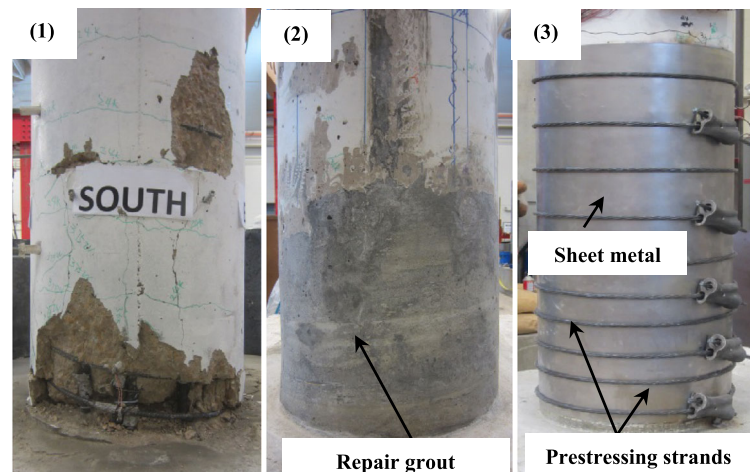**Fig. 3** Details of the studied prototype bridge.

Fig. 4 Details of the hybrid repair jacket: *1* damaged column, *2* original column cross section restored, *3* thin sheet metal wrapped around the column with prestressing strands placed over column.

only (Jirawattanasomkul 2013). Thus, due to the enhanced aggregate interlock provided, concrete shear strength in the hybrid jacketed column—similarly conventional steel jacketed column—is larger than that in column with prestressing strands (FRP or SMA) only.

4.2 Repair Techniques

Three different repair techniques were considered, including a CFRP repair jacket, a conventional thick steel repair jacket, and hybrid repair jacket (discussed in Sect. 4.1). The CFRP jacket was chosen as the first repair technique due to the excellent high strength-to-weight ratio which is becoming increasingly attractive for structural repair/retrofit projects (Priestley et al. 1996; Buckle et al. 2006; He et al. 2013; Grelle and Sneed 2013). The steel jacket was the first and the most widely used retrofit technique (Priestley et al. 1996; Buckle et al. 2006; ElGawady 2009; Fakharifar et al. 2013;), due to its availability, price, and ductile behavior when compared with FRP materials with brittle failure (Fakharifar et al. 2015c). However, in addition to the labor intense work required for steel plate or RC jacketing, one major concern, is the increase of the original cross section (i.e., increased stiffness and reduced natural vibration period (Haroun and Elsanadeby 2005) results in alteration of the system dynamic response). The additional flexural strength of a member with a thick repair jacket would increase the plastic shear demand on the retrofitted/repaired column. Thus, the conventional steel or RC concrete jackets need to be detailed so as not to trigger other failure modes such as cap beam damage or cause damage to other capacity protected elements (Priestley et al. 1996; Buckle et al. 2006; Fakharifar et al. 2014b). Therefore, active prestressing strands were considered as another repair technique. Active cables have the advantage of providing the
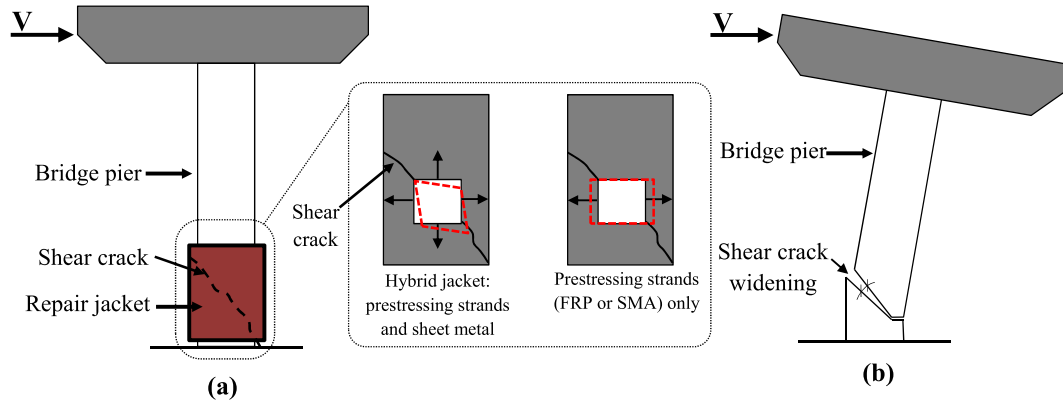
Fig. 5 **a** stress state in the repair jacket along the shear crack for confining pressure from hybrid jacket and prestressing strands, **b** increase of shear deformations due to widening of shear cracks in an RC column with existing damage subjected to aftershock attacks.

active confining pressure without increasing the column cross section (Saatcioglu and Yalcin 2003). However, tests proved that for retrofitted columns with prestressing strands, penetration of the prestressed cables into the cracked cover concrete caused loss of confining force in the active cables (Buckle et al. 2006). To incorporate the economical price of steel jackets with the benefit of active confining pressure, the hybrid confining jacket was proposed and considered as the third seismic repair intervention in this study.

4.3 Seismic Repair Design and Repair Performance Objectives

The bridge column repair design aimed at restoring the shear strength, providing the required confining pressure in the plastic hinge and inhibiting the lap splice failure. Repair jacket design procedure is briefly described as follow.

The height of plastic hinge to be repaired, L_{pz}, was calculated according to California Department of Transportation Seismic Provisions (CALTRANS 2004).

$$L_{pz} = \frac{3}{8} AR \times D \geq 1.5D \tag{1}$$

where AR is the column aspect ratio, and D is the column diameter.

The shear strength of the column was based on those of individual components and checked against the factored shear (Vosooghi and Saiidi 2012). That is,

$$\frac{V^o}{\phi} < V_c + V_s + V_j \tag{2}$$

where V^o is the base shear, $\phi = 0.85$, and V_c, V_s and V_j is the shear resisted by concrete, existing transverse reinforcement, and repair jacket, respectively. Due to unknown extent of damage from a MS event, the shear resistance of the concrete and spirals were neglected, and the repair jacket was designed to resist the shear demand.

The shear resistance for the different studied repair techniques was determined as follows (Priestley et al. 1996; Buckle et al. 2006; Vosooghi and Saiidi 2012).

$$V_{cj} = 0.5\pi t_j f_{cj} D \cot\theta \tag{3}$$

$$V_{sj} = 0.5\pi t_j f_{yj} D \cot\theta \tag{4}$$

$$V_{sp} = 0.5\pi A_{ps} f_{ps} D s^{-1} \cot\theta \tag{5}$$

where V_{cj}, V_{sj} and V_{sp} is the shear enhancement from CFRP jacket, steel jacket and prestressing strands, respectively; t_j is the jacket thickness (CFRP or steel); D is the column diameter; f_{cj} is the hoop stress in the CFRP jacket; f_{yj} is the steel jacket yield stress; A_{ps} is the cross sectional area of prestressing strand; f_{ps} is the level of prestressing stress in the strand; s is the vertical spacing between prestressing strands; and θ is the angle of the critical inclined shear-flexure crack to the column axis. For the hybrid repair jacket shear resistance was calculated as the contribution from both the steel jacket and the prestressing strands (i.e., $V_{sj} + V_{sp}$).

The required confining stress (f_l) to prevent the lap-splice failure (Priestley et al. 1996) for the substandard bridge was determined from Eq. (6).

$$f_l = \frac{A_b f_s}{\mu p l_s} \tag{6a}$$

$$p = \frac{\pi D'}{2n} + 2(d_b + c) \leq 2\sqrt{2}(d_b + c) \tag{6b}$$

where A_b is the cross sectional area of reinforcement bar, $f_s = 1.7$ times reinforcement yield stress ($=1.7f_y$), μ is the coefficient of friction (assumed as 1.4), l_s is the lap splice length, p is the crack surface perimeter, n is the number of longitudinal lapped bars, d_b is the reinforcement bar diameter, D' is the core diameter (outside to outside dimension of the circular transverse reinforcement), and c is the concrete cover thickness.

The required jacket thickness and spacing between prestressing strands to provide the adequate confining pressure in the plastic hinge region of damaged columns were calculated as follows (Priestley et al. 1996; Buckle et al. 2006).

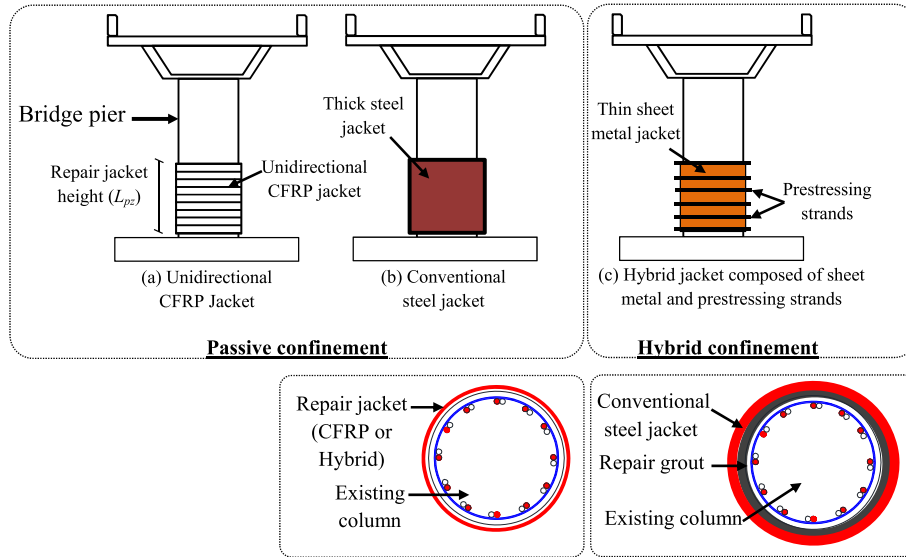$$t_{cj} \geq \frac{215D}{E_{cj}} \tag{7}$$

Fig. 6 Schematic of different repair techniques: **a** CFRP jacket, **b** conventional steel jacket, and **c** hybrid jacket.

$$t_{sj} \geq \frac{f_l D}{400} \tag{8}$$

$$s \leq \frac{A_{ps}(f_{ps} + 200)}{D} \tag{9}$$

where t_{cj} is the CFRP jacket thickness; t_{sj} is the steel jacket thickness; E_{cj} is the CFRP modulus of elasticity; and the remaining parameters were defined previously. The maximum spacing between the prestressing strands should not exceed six times the diameter of the longitudinal reinforcing bar (Buckle et al. 2006).

Figure 6 illustrates the schematic of the studied repair jackets. The jacket height for the studied repair techniques was calculated as $L_{pz} = 1220$ mm.

The CFRP jacket was assumed to have a tensile strength of 3800 MPa, modulus of elasticity of 227 GPa, and a rupture strain of 1.67 %. The selected composite CFRP repair system consisted of unidirectional high strength carbon fabric with fibers perpendicular to the column longitudinal axis (Fig. 6a). The required jacket thickness for the studied bridge column was calculated as 5.81 mm (using nominal fiber thickness).

A 7.5-mm thick A36 steel with minimum yield strength of 400 MPa was required for the thick steel repair technique. For practicality, a 10-mm thick steel jacket with yield strength of 400 MPa and modulus of elasticity of 200 GPa, with a 25 mm gap left between the column and the jacket to be filled with repair grout (Fig. 6b), was required.

For the hybrid jacket, the thin sheet metal with yield strength of 680 MPa; tensile strength of 771 MPa; and elastic modulus of 207 GPa was considered. Considering field-application and formability of the sheet metal around the existing column without specialized equipment in the field, a 1220 mm wide sheet with a thickness of 1.27 mm was calculated. The nominal 12 mm diameter seven-wire strands with the ultimate tensile strength of 1937 MPa and modulus of elasticity of 200 GPa were considered for repair

design. The spacing between strands and the required pre-stressing pressure in the cables were calculated as 1045 MPa and 100 mm, respectively (Fig. 6c).

5. Nonlinear Numerical Finite Element Modeling

An extensively calibrated—at the component and system level—nonlinear finite element model of the bridge is developed and subjected to sequences of MS-AS. The numerical FE models in this study were developed and analyzed using SeismoStruct nonlinear analysis program (Seismosoft 2013a). The program is capable of predicting the large displacement behavior of space frame structures under static and dynamic loading while taking into account both geometric nonlinearities (P-Δ effect) and material inelasticity (Ferracuti et al. 2009). The fiber based modelling approach using the 3D inelastic beam-column element discretized by uniaxial fiber elements was utilized to develop the numerical models. The applicable nonlinear fiber discretized beam/column elements calibrating parameters where computed according to the analytical column modeling strategies proposed by Berry and Eberhard (2007) and Haselton et al. (2008). Accuracy of the numerical models is significantly important for accurate and realistic assessment of the studied bridges during the MS-AS event. Many studies (Terzic and Stojadinovic 2013; Fakharifar et al. 2014c; Shamsabadi et al. 2009) have demonstrated the accuracy of adequately calibrated fiber elements in predicting the lateral force–displacement hysteresis relationship of different structural systems under static and dynamic loading conditions. Hilbert-Hughes-Taylor integration scheme (Scott and Fenves 2006) was utilized to acquire the global flexibility matrix for the flexibility based (FB) elements; considering the potential strain softening or localized deformations phenomena.

The Menegotto–Pinto (1973) steel model with Filippou et al. (1983) hardening rules and Fragiadakis et al. (2008)

additional memory rule for higher numerical instability/accuracy under transient seismic loading was used for the reinforcing steel material. To incorporate the accumulated damage from the MS in the longitudinal reinforcing steel (for simulated damaged column), the steel properties were modified (Vosooghi and Saiidi 2010, 2012) to consider the Bauschinger effect (Kent and Park 1973), which resulted in lowering the reversed yield stress and the reversed stiffness. For concrete the nonlinear variable confinement model of Madas and Elnashai (1992) with Martinez-Rueda (Martinez-Rueda and Elnashai 1997) cyclic rules was used. The variable confinement algorithm enables the explicit computation of relation between the concrete lateral dilation and straining of the transverse reinforcement computed at every analysis step. The Ferracuti and Savoia (2005) model was utilized as the FRP confined concrete model. This model follows the constitutive relationship and cyclic rules proposed by Mander et al. (1988) and Yankelevsky and Reinhardt (1989) under compression and tension, respectively. This model implements the Spoelstra and Monti (1999) model for the confining effect of FRP wrapping. The FRP material was modelled as linear elastic material up to rupture with no compressive strength.

5.1 Nonlinear Numerical Model Details

The fiber discretized cross section of a numerical RC column and representative stress–strain behavior associated to fibers are shown in Fig. 7. For confined core fibers either steel-confined (for thick steel and hybrid jackets), or FRP-confined would be considered. Column elements were modelled through inelastic frame elements. The effect of lap-splice reinforcement was desired to be somewhat represented in the numerical models hysteresis behavior. For RC columns with spliced reinforcement, a multilinear smooth polygonal hysteresis loop, developed in the work of Sivaselvan and Reinhorn (1999, 2001) through a zero length rotational spring (available in Seismostruct) could be used to

model the plastic hinge to include the hysteresis pinching associated with reinforcement slippage. However, the state of rebar stress at splice failure was needed to be determined. FEMA 356 (2000) provisions on lap-spliced bars was used to determine the rebar stress at failure, however the predicted response was not accurate especially in the post-peak degrading behavior. Study by Cho and Pincheira (2006) indicated that FEMA 356 underestimates the lapped rebar stress. Using bond-slip models are a proven method for inelastic analysis of RC columns with lap-splice failure (Xiao and Ma 1997; Harajli et al. 2002; Cho and Pincheira 2006). However, bond-slip model could not be directly incorporated in the numerical model, since a zero length stress–displacement section was not available. Besides, the effect of the lateral confining pressure from different repair jackets was also important. To achieve this, the stress–strain relationship of the longitudinal steel reinforcement for lap spliced reinforcement was reduced to simulate the expected backbone of lateral force–displacement relationship. It's noteworthy to mention that the Xiao model (Xiao and Ma 1997) could be used to establish the average bond stress–lateral displacement relationship for columns with lap-spliced reinforcement in the as-built and with the consideration of the lateral confining pressure conditions in retrofitted ones, and then reduce the steel properties accordingly. When ignoring the lap-splice, monotonically increasing lateral force–displacement relationship with ascending post-peak behavior was observed. However, reduced material properties captured the bar-pullout and the associated softening behavior evident from lap-spliced columns hysteresis behavior. The method used was approximate, however resulted in fairly accurate predictions of the numerical models, as shown later in the paper. Note that fiber discretized sections with uniaxial constitutive laws were used in the finite element model and the fiber element is incapable of accurately aggregating shear deformations. However, the studied columns in the current investigation constitute
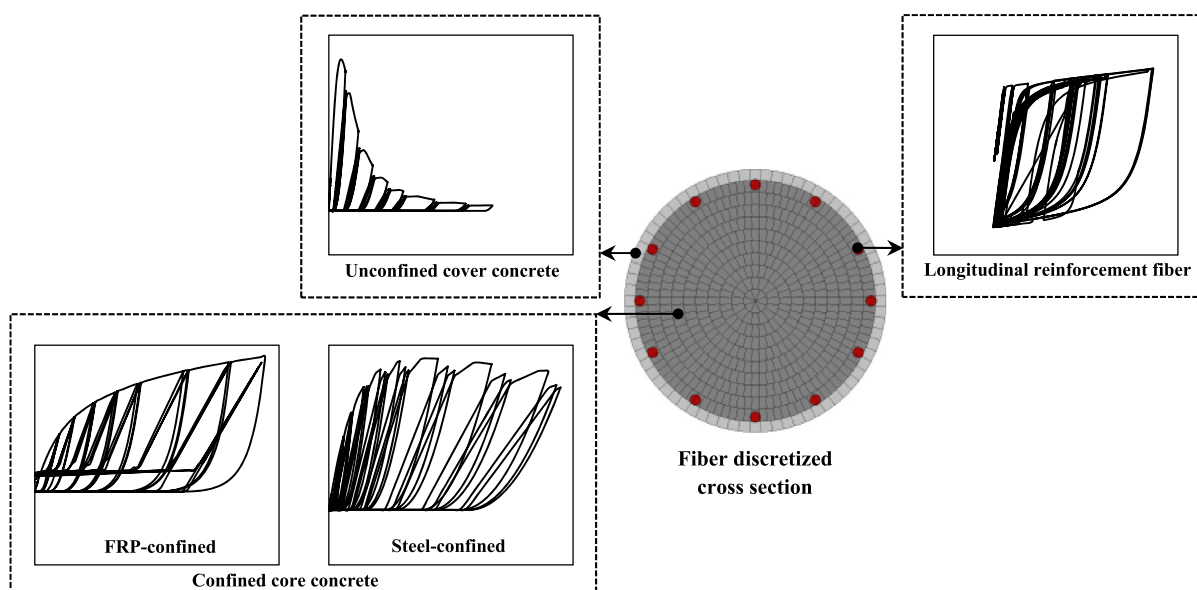

Fig. 7 Representative stress–strain responses of material fibers in an RC column cross section.
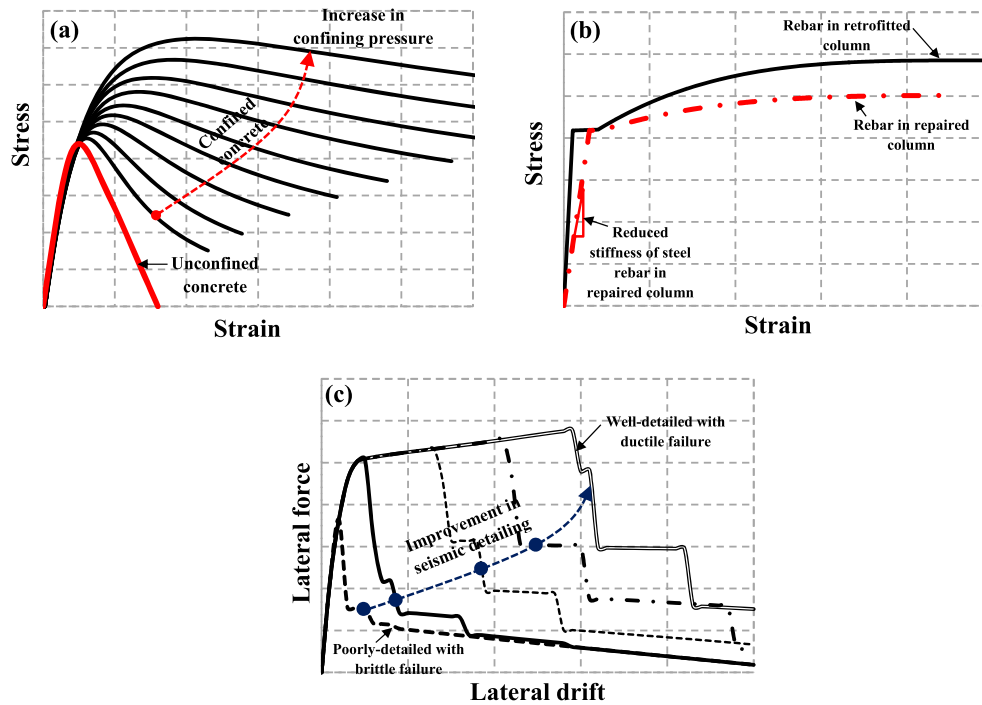
Fig. 8 Representative constitutive models and lateral force–drift relationship: **a** unconfined and confined concrete model, **b** stress state in steel reinforcement in retrofitted and repaired column, and **c** lateral force–drift responses according to seismic reinforcement detailing.

primarily flexural dominant (column aspect ratio well above 2.5) hysteresis response.

The increase of lateral confining pressure on the constitutive confined concrete model in this study is illustrated in Fig. 8a. A typical stress–strain relationship for the virgin steel reinforcement versus damaged reinforcement is illustrated in Fig. 8b. For the retrofit case, the jacket is applied on the intact column cross section prior to any major event, while for the repair scenario the repair jacket is implemented after column experiences some extent of damage. As it can be seen, in the case of a repaired column the initial stiffness of steel reinforcement is reduced, as well as the post-yield strain hardening. Representative lateral force-drift relationship for an identical RC column depending on the reinforcement detailing, is also illustrated in Fig. 8c. It can be seen brittle failure could be avoided through inclusion of seismic reinforcement, such as external jackets.

5.2 Verification of Numerical Models with Experimental Test Results

Extensive verification of the numerical models for their capability of capturing and simulating the global and local forces and deformations were implemented first. The authors have also verified their analytical models for FRP jacketed concrete columns under both monotonic and dynamic timehistory loading elsewhere (Fakharifar et al. 2014c). To evaluate the accuracy of the developed numerical models for evaluating the behavior of bridges subjected to MS-AS sequences, experimental models were selected from full scale RC column/bridge structures subjected to multiple series of ground motions.

Experimental tests on RC columns tested under incrementally increasing reversed cyclic loading and constant axial load with lap spliced reinforcement ($l_s = 20d_b$) as part of another study by the authors was selected to evaluate the accuracy of the developed numerical models in predicting the force–displacement relationship of columns with lap-spliced reinforcement. Figure 9a depicts backbone of the predicted force–displacement relationship from the numerical model versus experimental test results. It is clear that, ignoring the slip effect would not capture post-capping degradation in the numerical model. However, the reduced steel allows capturing the post-peak strength degradation.

An RC cantilever column with continuous reinforcement (Column BG-2) tested under constant axial load and unidirectional quasi-static incrementally increasing lateral displacement up to failure was selected (Saatcioglu and Grira 1999). The selected column was chosen for verification since unlike regular RC columns with stirrups or spirals, welded reinforcement grids were used as confinement reinforcement. Therefore the equivalent confining pressure from the grids was considered in the model. Figure 9b indicates the high accuracy of the numerical model in predicting the hysteretic behavior of the experimental column specimen in terms of strength, stiffness and displacement capacity. Besides, it was concluded that alternative forms of confinement can also be considered in the numerical analysis, as long as the appropriate lateral confinement pressure is provided in the model.

A full-scale RC bridge pier subjected to series of six incremental ground motions developed by PEER and NEES (PEER 2010) as part of a blind prediction contest was
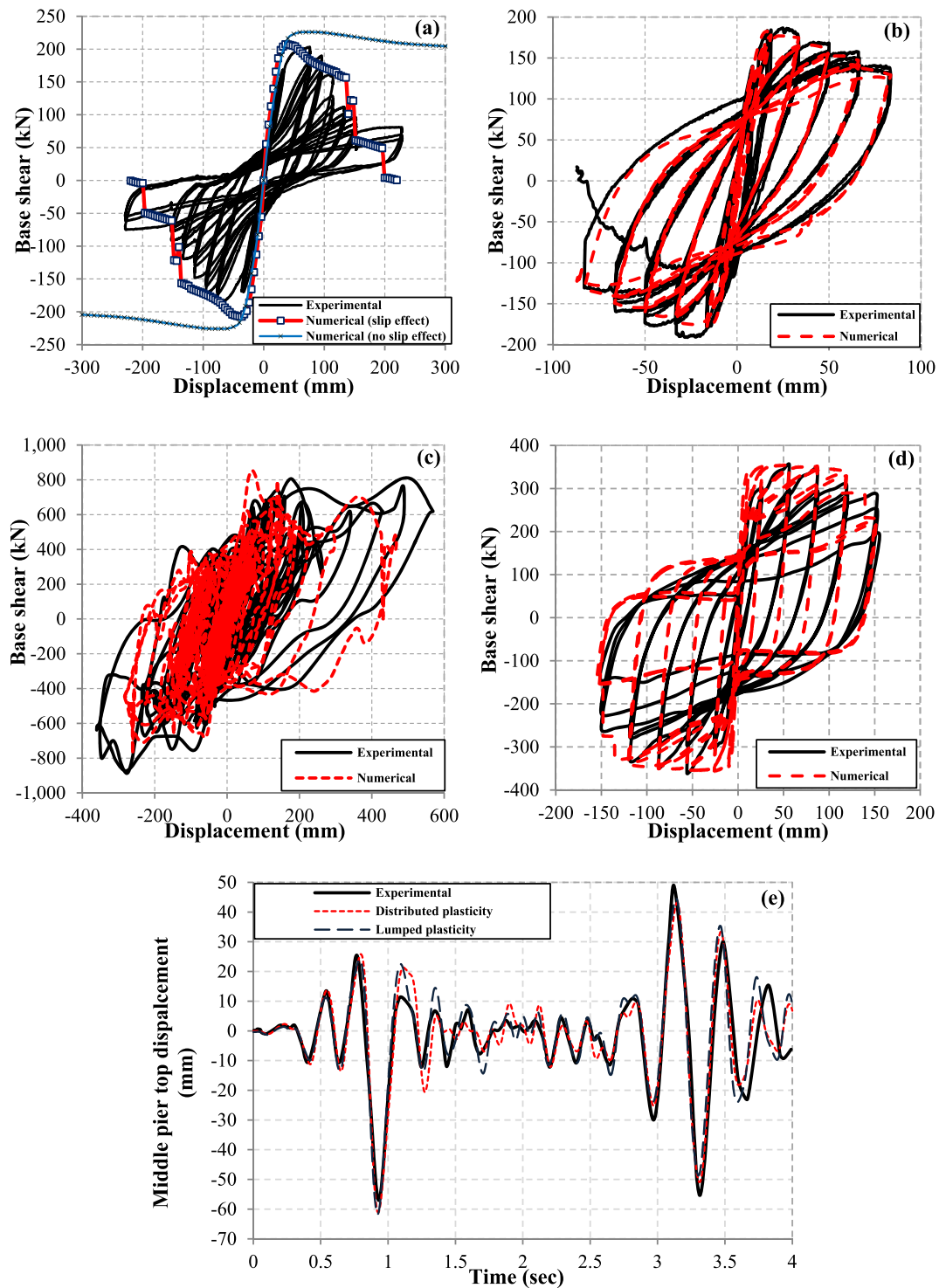
Fig. 9 Comparison of numerical models versus different experimental test specimens: **a** RC column with lap-spliced reinforcement under cyclic load reversals, **b** RC column under cyclic load reversals (Saatcioglu and Grira 1999), **c** RC column under shake table test (PEER 2010), **d** concrete-filled steel tube column under cyclic load reversals (Marson and Bruneau 2004), **e** full scale bridge shake table test (Pinto et al. 1996), **f** A2, **g** A4, **h** A8; and **i** A10 column specimens (Kunnath et al. 1997).

selected. The input ground motions commenced with the low intensity excitations succeeded by high intensity motions to bring the bridge pier to the incipient collapse state. The numerical model was verified adopting the proposed recommendations by Bianchi et al. (2011). Figure 9c demonstrates the capability of the numerical model in reproducing the dynamic hysteresis behavior of the studied

bridge pier. The selected bridge pier specimen exhibits significantly high level of nonlinearity (both material inelasticity and geometric nonlinearity). Damage was observed in the form of concrete spalling, concrete cracking, longitudinal bar buckling (thirteen of the eighteen bars were buckled), and longitudinal bar fracture in the plastic hinge region formed at column-footing interface (Schoettler et al. 2012).
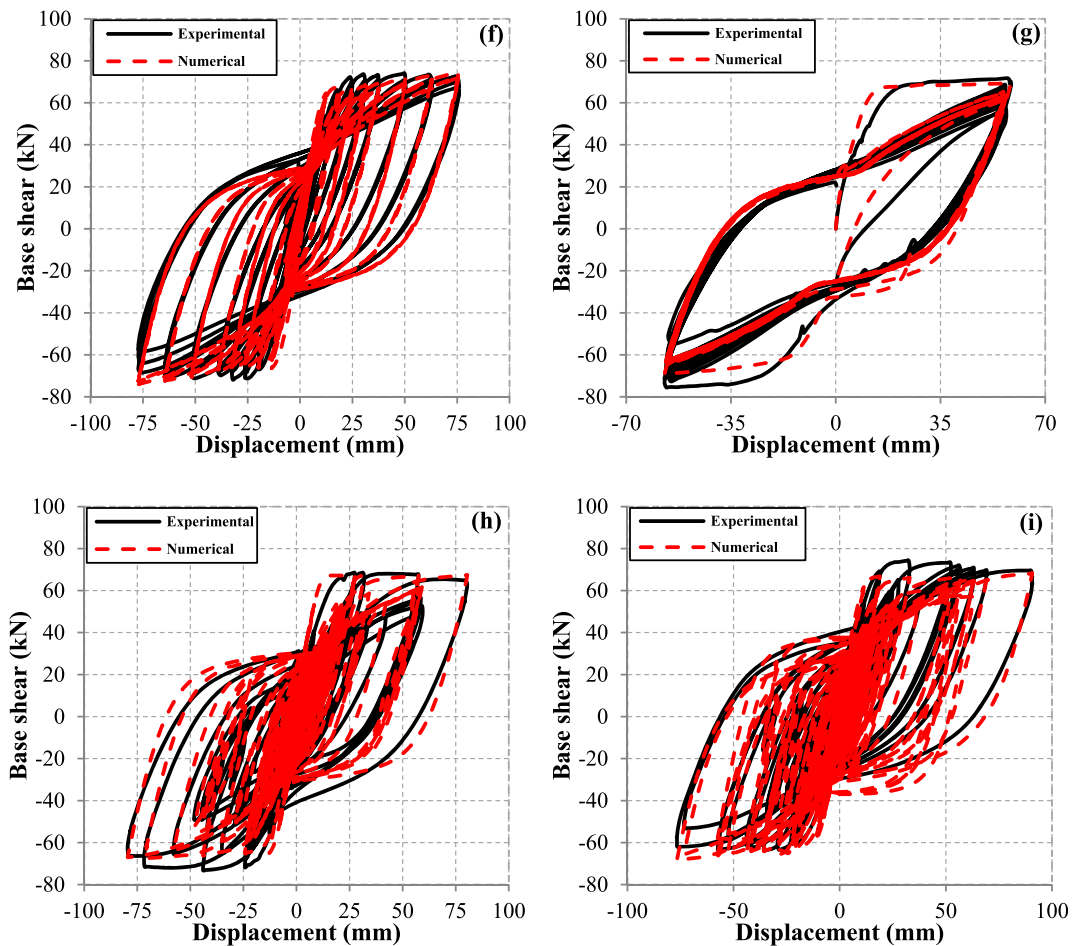
Fig. 9 continued

The numerical model could successfully capture the seismic response of the pier specimen subjected to six seismic sequences of various intensities.

To evaluate the adequacy of the developed numerical models in the case of steel-jacketed RC columns, a full scale concrete-filled steel tube bridge pier under incrementally increasing reversed cyclic loading and constant axial load (Marson and Bruneau 2004) was selected. Figure 9d depicts the predicted force–displacement relationship of the numerical model with reasonable accuracy as compared to the experimental test results.

To evaluate the accuracy of the numerical models in predicting the system response, the large scale bridge specimen tested in pseudo-dynamic type test was selected (Pinto et al. 1996). The bridge specimen was subjected to two successive input motions on shake table tests, including the design earthquake, followed by the 1.2 times the design level earthquake. The bridge deck was modelled using elastic frame elements with mass lumped along the centerline (Seismosoft 2013b). Both distributed plasticity (inelastic distributed element) and lumped plasticity (inelastic plastic hinge element) elements were adopted to model the bridge columns. The predicted displacement time history of the middle pier from the distributed plasticity and lumped plasticity models are compared versus experimental results in Fig. 9e. The results indicate the adequacy of both types of

element formulations in predicting the displacement time history and the maximum displacement with reasonable accuracy.

Finally, to further evaluate the accuracy of the developed numerical models under cumulative seismic damage (expected for MS-AS), series of RC bridge column specimens tested under various loading histories were chosen (A2, A4, A8 and A10 column specimens) (Kunnath et al. 1997). Each of the selected bridge column specimens were tested under a constant axial load and a unique lateral load path, specifically, specimen A2: standard cyclic load with three full symmetric cycles at increasing ductility up to failure; specimen A4: constant amplitude reversed cyclic displacement of $\pm 3\Delta y$ (Δy = yield displacement level); specimen A8: random earthquake displacement histories, representing four scenario earthquake sequence (minor, minor, damaging and severe earthquakes), and A10: representing five scenario earthquake sequence (major, minor, moderate, minor and severe earthquakes) (Kunnath et al. 1997). Comparison of calculated force–displacement relationship of the studied column specimens against experimental results are illustrated in Fig. 9f–i for A2, A4, A8 and A10 column specimens, respectively. The obtained results indicate the high accuracy of the numerical models to simulate the obtained experimental results under different loading histories—including multiple earthquakes—in terms of strength, stiffness

and ductility. The developed numerical models exhibited to provide sufficient accuracy, and these modeling assumptions were adopted for performance-based evaluation of the bridge in the current study.

6. Incremental Dynamic Analysis

The nonlinear static procedure, commonly referred to as static pushover analysis (SPA) has become a standard method to estimate seismic deformation demands in structures as well as their local and global capacities (Villaverde 2007). However, the SPA lacks a rigorous theoretical foundation, based on the incorrect assumption "that the nonlinear response of a structure can be related to the response of an equivalent single-degree-of-freedom system" (Villaverde 2007). The inherent inability of SPA analysis to correctly identify the seismic demands, specifically for structures that deform far into their inelastic range of behavior (expected for structures subjected to MS-AS sequence) has been clearly signified in many studies (Ferracuti et al. 2009; Villaverde 2007; Chopra and Goel 2002; Fakharifar et al. 2015c; amongst others). Therefore, incremental dynamic analysis (IDA), developed by Vamvatsikos and Cornell (2002), was incorporated to accurately evaluate the demand and capacity of the studied repaired bridges under different set of MS-AS sequences. IDA is capable of accurately estimating the failure/collapse capacity of structures subjected to seismic excitations of different intensities (Villaverde 2007; Vamvatsikos and Cornell 2002). An IDA requires multiple series of nonlinear dynamic time history analysis (NTHA) of the structure subjected to incrementally increasing ground motion intensity. The IDA analysis starts from a very low (non-negative) scaling factor multiplied by the intensity measure (IM) of each unscaled ground motion time history. The scaling factor for each run is incrementally increased until the structural median collapse (or until a defined failure limit state) is reached. Each data point on the IDA curve corresponds to a single NTHA for the structure subjected to one ground motion time history scaled to one intensity level. This procedure is repeated to obtain all the data points—from elastic to inelastic and finally to global dynamic instability (or numerical non-convergency)—for the full range of IDA curves.

The use of PGA as the IM for the structures with dominant first mode of vibration may result in biased structural response predictions (Vamvatsikos and Cornell 2002). For structures with a moderate period of vibration with maximum drift ratio as the damage measure (DM) and the 5 % damped first mode spectral acceleration (Sa (T1,5 %)) as the IM subjected to a bin of relatively moderate to large magnitudes, M, results obtained from scaled and un-scaled records are similar. The use of Sa (T1) as the IM is often recommended (Vamvatsikos and Cornell 2002; Tehrani and Mitchell 2013), and was adopted in this study.

Engineering demand parameter (EDP) is the output of the IDA analysis that elicits the state of structural damage in terms of its response under different earthquake records. For brevity, the IDA results are presented only in terms of maximum drift ratio as the demand parameter.

6.1 Damage/Limit State

Four damage states, namely minor, moderate, extensive and collapse as defined by HAZUS-MH (2003) were adopted herein, in which they were correlated with the quantitative engineering demand parameters. The drift-based limit states developed by Dutta and Mander (1998) were adopted to define the bridge columns drift limits. The drift limits considered for the bridge columns were 0.005, 0.007, 0.015, 0.025 and 0.05 for no damage, minor, moderate, extensive and collapse damage states, respectively. However, the constant drift limits better serve as a global (system) response quantity. For a more accurate evaluation, the strain limit sates (local response quantity) developed by Priestley et al. (2007) were incorporated as well. Using moment curvature and pushover analysis the strain limits were related to drift limit states. The maximum compressive strain in the confined core concrete and the maximum tensile strain in the longitudinal reinforcing steel were considered as the strain-based limit states (Priestley et al. 2007).

The bar buckling and bar fracture damage states were calculated according to the equations developed by Berry and Eberhard (2007). The equation proposed by Mackie and Stojadinovic (2007) for calculating the drift at column failure (i.e., lateral drift level beyond the peak strength that column reaches zero strength) was adopted to define the complete failure limit state. Incorporating the effect of load history on reinforcement bar buckling limit state—as shown in past studies (e.g., Rodriguez et al. 1999)—under the first seismic event may significantly alter the obtained results for the subsequent seismic event. Nevertheless, effects of seismic load-path history on reinforcement bar buckling were not considered.

6.2 Mainshock-Aftershock Seismic Ground Motion Records

The ground motions were selected from the Pacific Earthquake Engineering Research Center (PEER) Strong Motion Database, specifically, from the study by Baker et al. (2011) providing several standardized sets of ground motions for the PEER's Transportation Research Program. The selected ground motions are neither site-specific nor structure specific (i.e., unbiased) (Baker et al. 2011). The earthquake ground motions records in this study include both type of far-fault (also referred to as far-field) and near-fault records.

Two bins of earthquake records were considered to generate the MS-AS sequences, namely, ensemble 1 and ensemble 2. Ensemble 1 constitutes far-fault records where ensemble 2 included records with near-fault effects. Each ensemble constitutes records of large and moderate magnitude. The acceleration response spectra of ensemble 1 and 2 record sets (unscaled) are illustrated in Fig. 10.
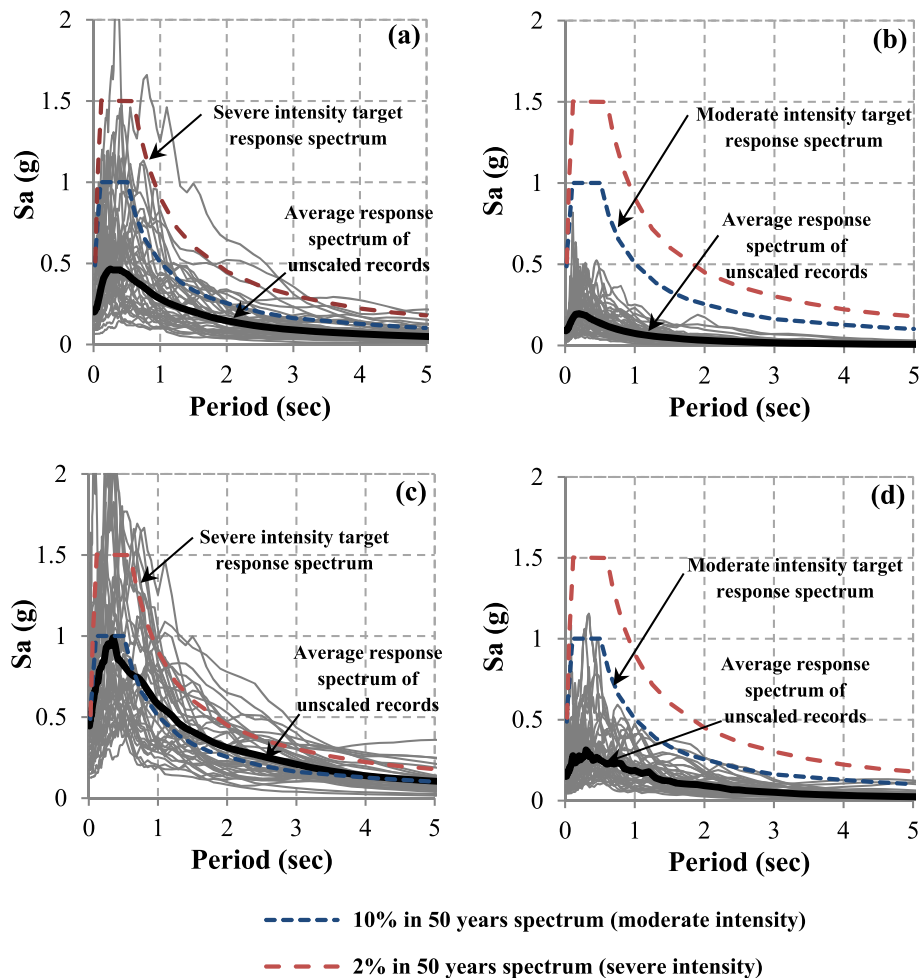
Fig. 10 Response spectra of selected unscaled ground motions and different hazard levels target response spectra: **a** ensemble 1 large (severe) magnitude, **b** ensemble 1 moderate magnitude; and **c** ensemble 2 large (severe) magnitude, **d** ensemble 2 moderate magnitude.

Two seismic sequences from ensemble 1 and two seismic sequences from ensemble 2 were considered, namely (1) severe MS-moderate AS, and (2) severe MS-severe AS. Eighty MS-AS seismic sequences from the ensemble 1 and eighty MS-AS seismic sequences from the ensemble 2 record sets were generated. Subsequently, for each ensemble, records were selected from the corresponding intensity record set. For instance for severe MS-moderate AS from ensemble 1, large magnitude (response spectra in Fig. 10a) and moderate magnitude (response spectra in Fig. 10b) records were paired. Similarly, for severe MS-severe AS from ensemble 1, large magnitude records followed by the same set of records were paired. Similar seismic sequences were generated from ensemble 2 bin of records. No paired seismic sequence from ensemble 1 to 2 and opposite were considered (i.e., no near fault MS-far fault AS or opposite). Hence, total of 160 paired accelerations (40 severe MS-moderate AS and 40 severe MS-severe AS from ensemble 1 and 2) were generated.

To simulate the free vibrating response of the bridge at the end of the MS, 20 s of zero acceleration was introduced between the MS and AS acceleration time histories, to assure that the bridge was at rest prior to the AS event.

For each intensity level, the selected ground motions were scaled to match the Los Angeles-California site response spectrum for two different hazard levels, namely 10 % probability of exceedance in 50 years (moderate earthquake), and 2 % probability of exceedance in 50 years (severe earthquake) (Fig. 10). The target response spectra were utilized to scale the original records at each intensity level. The selected unscaled ground motions from the severe (Fig. 10a) and moderate (Fig. 10b) intensity record sets from ensemble 1 were scaled considering the 2 and 10 % in 50 years target response spectra, respectively, to calculate the scaled severe and moderate magnitude records for ensemble 1. The same procedure was adopted to scale the original records from the ensemble 2 set of records. The characteristics of ensemble 1 and 2 record sets are detailed below.

Ensemble 1 (far-fault): for this set the large magnitude suite of records consists of 40 broad-band ground motions that their response spectra match the median and log standard deviations predicted for a large magnitude ($M_w = 7$) strike-slip earthquake at a distance of 10 km. The moderate magnitude motions constitutes 40 broad-band ground motions with their response spectra matching the median and log standard deviations predicted for a moderate magnitude
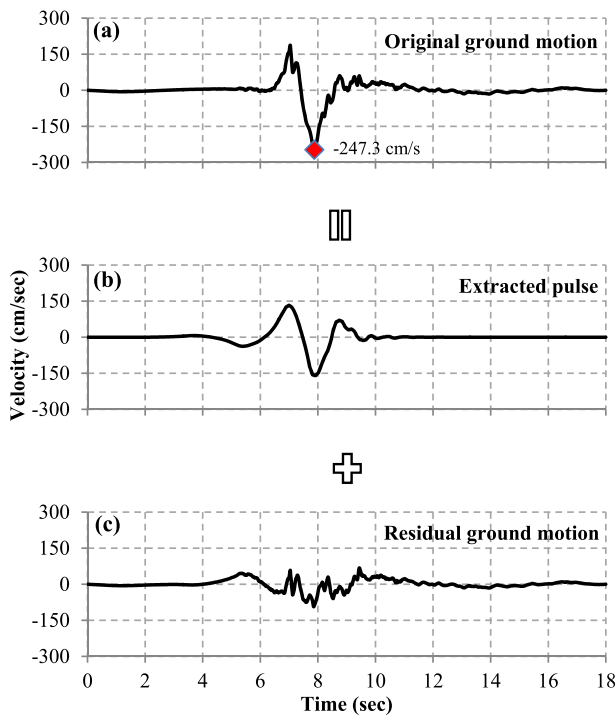
Fig. 11 A near-fault ground motion with large velocity pulse from ensemble 2 record set: **a** original ground motion, **b** extracted pulse, **c** and residual motion.

($M_w = 6$) strike-slip earthquake at a distance of 25 km. The selected set of ground motions as the far fault records represent a very broad range of spectral amplitudes up to two orders of magnitude. These set of records cover a broad range of intensities at sites located near active crustal earthquake sources (Baker et al. 2011). The acceleration response spectra of the severe and moderate intensity records from ensemble 1 ground motions are presented in Fig. 10a, b. Detailed information on the adopted records can be found elsewhere (Baker et al. 2011).

Ensemble 2 (near-fault): For this set the large magnitude ground motions consists of 40 records containing strong velocity pulses of varying periods. The velocity pulses are typically observed in the near fault ruptures due to directivity effects. This set of records are somewhat intense that constitute motions having a strike parallel peak ground velocity up to 250 cm/s. Figure 11 illustrates one original ground motion with strong velocity pulse along with the extracted pulse and non-pulse (residual) part of the original motion. The moderate magnitude ground motions consist of 40 records each obtained from scaling the large magnitude records (Bearman 2012). The acceleration response spectra of the ensemble 2 ground motions are presented in Fig. 10c, d. These set of near fault motions are similar to near-fault motions included in ATC-63 (2009), except these motions have a variety of pulse periods (1–12.9 s). This is important, since the pulse period, relative to the period(s) of vibration of a structure is not negligible. Besides, these set of records are somewhat intense that constitute motions having a strike parallel peak ground velocity of 250 cm/s (see Fig. 11a).

6.3 IDA Analysis Results Under Severe MS-Severe AS and Discussion

For brevity results from an extensive series of IDA analyses are presented only in terms of structural collapse capacity and maximum drift. For each series of analyses four cases of the studied bridge were considered: unrepaired bridge, column repaired with CFRP jacket, column repaired with conventional steel jacket, and column repaired with hybrid jacket. Each individual IDA curve corresponds to one MS-AS pair of ground motion. The IDA results were utilized to construct the IDA curves under back-to-back time histories. Extensive data from IDA analyses were generated and the IDA curves only for the severe MS-severe AS are plotted in Fig. 12. The IDA results under the severe MS-moderate AS are summarized at the end of this section.

The IDA results for the unrepaired case and the CFRP, conventional steel and hybrid repair cases subjected to severe MS-severe AS of ensemble 1 bin of records are presented in Fig. 12a–d, respectively. Similarly, IDA results under severe MS-severe AS from ensemble 2 suite of records for the unrepaired, CFRP, conventional steel and hybrid repaired cases are presented in Fig. 12e–h, respectively. To evaluate the impact of damage from the MS-AS sequence compared to an MS event only, the median of IDA results for the bridge subjected to severe MS only (i.e., no AS event) is superimposed on Fig. 12a, e accordingly (red dotted line).

The obtained mean structural collapse capacity for the MS only compared to MS-AS (Fig. 12a, e) is reduced as from 0.83 to 0.33 g; and from 0.69 to 0.36 g, for the ensemble 1 and 2 bin of records, respectively (60.0 and 47.8 % reduction in mean structural collapse capacity, respectively). This observation clearly indicates the effect of existing damage under a severe MS on the post-MS collapse capacity when severe AS is considered. Similarly, the obtained mean maximum drift level that the bridge could sustain prior to collapse for the MS only compared to MS-AS (Fig. 12a, e) is reduced from 3.42 to 2.35 %; and from 3.33 to 2.58 %, for the ensemble 1 and 2 bin of records, respectively (31.3 and 22.5 % reduction in maximum attainable drift level prior to collapse, respectively). The obtained mean structural collapse capacity/maximum drift for the original bridge subjected only to one seismic event (i.e., no AS) reveals the unsatisfactory performance of the bridge column with lap-splice deficiency, as expected. The original bridge could not reach drift capacity recommended by different seismic codes of practice (e.g. CALTRANS 2004). It is also shown that the accumulated damage under severe MS had impact on the post-MS collapse strength/deformability of the MS-damaged bridge when subjected to severe AS.

Usually the term MS-AS implies a severe MS followed by a minor/moderate AS, and the presented results herein is an extreme scenario, where the first severe earthquake is succeeded by another severe earthquake. Hence, the obtained results may not be realistic and represent the lowest bound to the mean structural collapse capacity. It is unlikely a severe MS is followed by a similar severe AS.
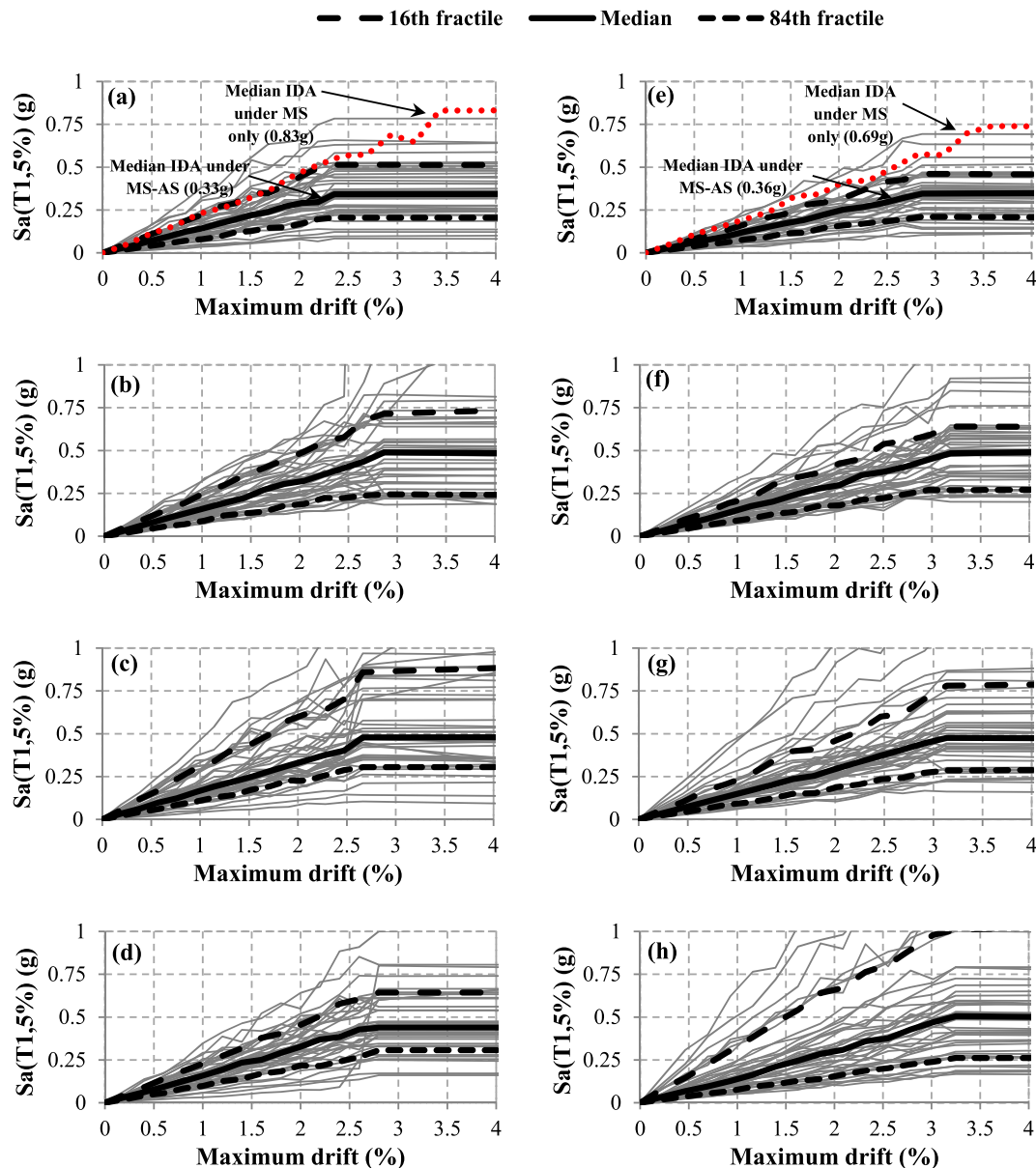
Fig. 12 IDA results (maximum drift) of the studied bridge under severe MS-severe AS sequence: ensemble 1 records **a** unrepaired, **b** CFRP, **c** conventional steel, and **d** hybrid; ensemble 2 records **e** unrepaired, **f** CFRP, **g** conventional steel, **h** hybrid jacket.

The mean structural collapse capacity for the CFRP, conventional steel, and hybrid repaired bridge columns under severe MS-severe AS from ensemble 1 record set (Fig. 12b–d) was 0.47, 0.48 and 0.43 g, respectively [i.e., 42.4, 45.5 and 30.3 % increase in the structural mean collapse capacity, respectively, compared to the unrepaired bridge (0.33 g)]. Similarly, the mean structural collapse capacity for the CFRP, conventional steel, and hybrid repaired bridge columns under the severe MS-severe AS from ensemble 2 record set (Fig. 12f, h) was 0.5, 0.46 and 0.5 g, respectively [i.e., 38.8, 27.7 and 38.8 % increase in the mean structural collapse capacity, respectively, compared to the unrepaired bridge (0.36 g)]. The obtained mean structural collapse capacities for the repaired bridge indicate the efficacy of confining repair jackets to be significant (up

to 45.5 %) for the post-MS collapse capacity of the earthquake-damage bridge.

Similar results on significance/necessity of repair jackets application were found for the severe MS-moderate AS sequences. However, the decrease in the mean structural collapse capacity between the MS only and severe MS-moderate AS was less significant compared to the severe MS-severe AS case. It is due to the fact that the major/primary damage is accumulated during the higher intensity seismic event, either during the FS or AS, and not depending on the sequence of events. For this reason, repair jackets were less effective for the severe MS-moderate AS compared to severe MS-severe AS sequence. The repair jackets were still required for the severe MS-moderate AS sequence as lapped reinforcement bars are seismically deficient in the

plastic hinge region. The results under severe MS-moderate AS seismic sequences confirm that the primary damage occurred under the severe MS and not the moderate AS, but numerous inelastic excursions are critical for lap-spliced columns even when subjected to minor or moderate AS. For instance, checking some of the steel reinforcement fibers stress–strain histories under single seismic event indicated the steel linear response up to proximity of yielding. However, same fiber under two seismic events exhibited highly nonlinear (post-yield) stress–strain response.

Comparison of Fig. 12a, e indicate that the mean structural collapse capacity of the original bridge under MS-only from ensemble 2 (near-fault) is smaller compared to ensemble 1 (far-fault) (0.69 g for near-fault records versus 0.83 g for far-fault records). The forward directivity effect and permanent displacement effect resulting in long period and large velocity pulse of near-fault ground motions (e.g. Fig. 11) have been addressed in previous studies.

The abovementioned results clearly indicate that the CFRP, steel and hybrid repair jackets were essential for post-MS collapse resilience of earthquake damaged bridge piers subjected to potential aftershocks of moderate or severe intensity. However, the repair jackets were most effective for the severe MS-severe AS scenario, and conversely were least effective for severe MS-moderate AS. Overall, the obtained results prove the efficacy of the studied repair jackets on post-MS seismic resilience of substandard RC bridge piers under aftershocks.

7. Fragility Analysis of the Bridge

Eventually, a probabilistic seismic demand model (PSDM) was developed for the fragility curves for the studied bridge. Seismic fragility curves describe the likelihood of exceeding the capacity of the bridge structures under a given level of strong ground motion. Fragility curves were developed to assess the vulnerability of the as-built and repaired bridge under back-to-back MS-AS sequences and select the optimal repair technique for MS-damaged bridge piers subjected to aftershocks. The PSDM establishes a correlation between the EDPs and ground IMs. The PSDM model is regarded as the most rigorous and reliable analytical method to derive fragility functions (Shinozuka et al. 2000; Billah et al. 2013). The cloud approach (Nielson and DesRoches 2007) was used to develop the PSDM model utilizing the IDA results. Fragility curves for two intensities of MS-AS, namely severe MS-severe AS and severe MS-moderate AS are developed for four damage states, namely slight, moderate, extensive and collapse. Regression analyses were undertaken to acquire the mean and standard deviation for each damage state, by assuming the power law model as suggested by Cornell et al. (2002), which derives a logarithmic correlation between median EDP and the selected IM.

$$EDP = a(IM)^b \qquad (10)$$

where a and b is the unknown coefficients estimated from the regression analysis of the response data points from IDA

results. The intermediate responses from the IDA results were required, as the IDA analyses established the response from low to high levels of ground motion intensities. The relation by Baker and Cornell (2006) was adopted to estimate the dispersion of the demand, $\beta_{EDP|IM}$, conditioned upon the IM.

$$\beta_{EDP|IM} = \sqrt{\frac{\sum_{i=1}^{N} (\ln(EDP) - \ln(aIM^b))^2}{N-2}} \qquad (11)$$

where N is the number of total analyses cases.

By having the PSDMs and the limit states at different damage states the fragilities were obtained from Eq. (12) (Nielson and DesRoches 2007) as follows.

$$P[LS|IM] = \Phi \left[\frac{\ln(IM) - \ln(IM_n)}{\beta_{comp}} \right] \qquad (12)$$

where Φ is the standard normal cumulative distribution function; IM_n is the median value of the IM; and $\ln(IM_n)$ is the natural log of the median value of IM for the selected damage state (e.g. minor, moderate, extensive and collapse) as shown in Eq. 13 (Billah et al. 2013).

$$\ln(IM_n) = \frac{\ln(S_c) - \ln(a)}{b} \qquad (13)$$

where a and b is the regression coefficients of the PSDMs; and β_{comp} is the dispersion component as shown in Eq. (14) (Nielson and DesRoches 2007).

$$\beta_{comp} = \frac{\sqrt{\beta_{EDP|IM} + \beta_c^2}}{b} \qquad (14)$$

where S_c is the median and β_c is the dispersion value of the unrepaired/repaired bridge capacity, as the lognormal parameters for the damage states.

7.1 Fragility Analyses Results and Discussion

The fragility curves for the studied bridge in the repaired and unrepaired condition under severe MS-severe AS set of records from ensemble 1 (far-fault) and ensemble 2 (near-fault) for minor, moderate, extensive and collapse damage states are presented in Fig. 13a–h, respectively (Fig. 13a–d for ensemble 1 and Fig. 13e–h for ensemble 2). Similarly, the results under severe MS-moderate AS sequences from ensemble 1 and 2 for minor, moderate, extensive and collapse damage states are presented in Fig. 14a–h, respectively.

The obtained fragilities indicate that the fragility curves for the unrepaired scenario almost overlaps the repaired cases under the slight damage state, where the extent of damage is somewhat negligible (i.e., the damage state is cosmetic and repairable, and the onset of bar buckling did not occur). All the fragility curves irrespective of the repair jacket material, intensity of seismic sequences (i.e., severe MS-severe AS or severe MS-moderate AS) and earthquake
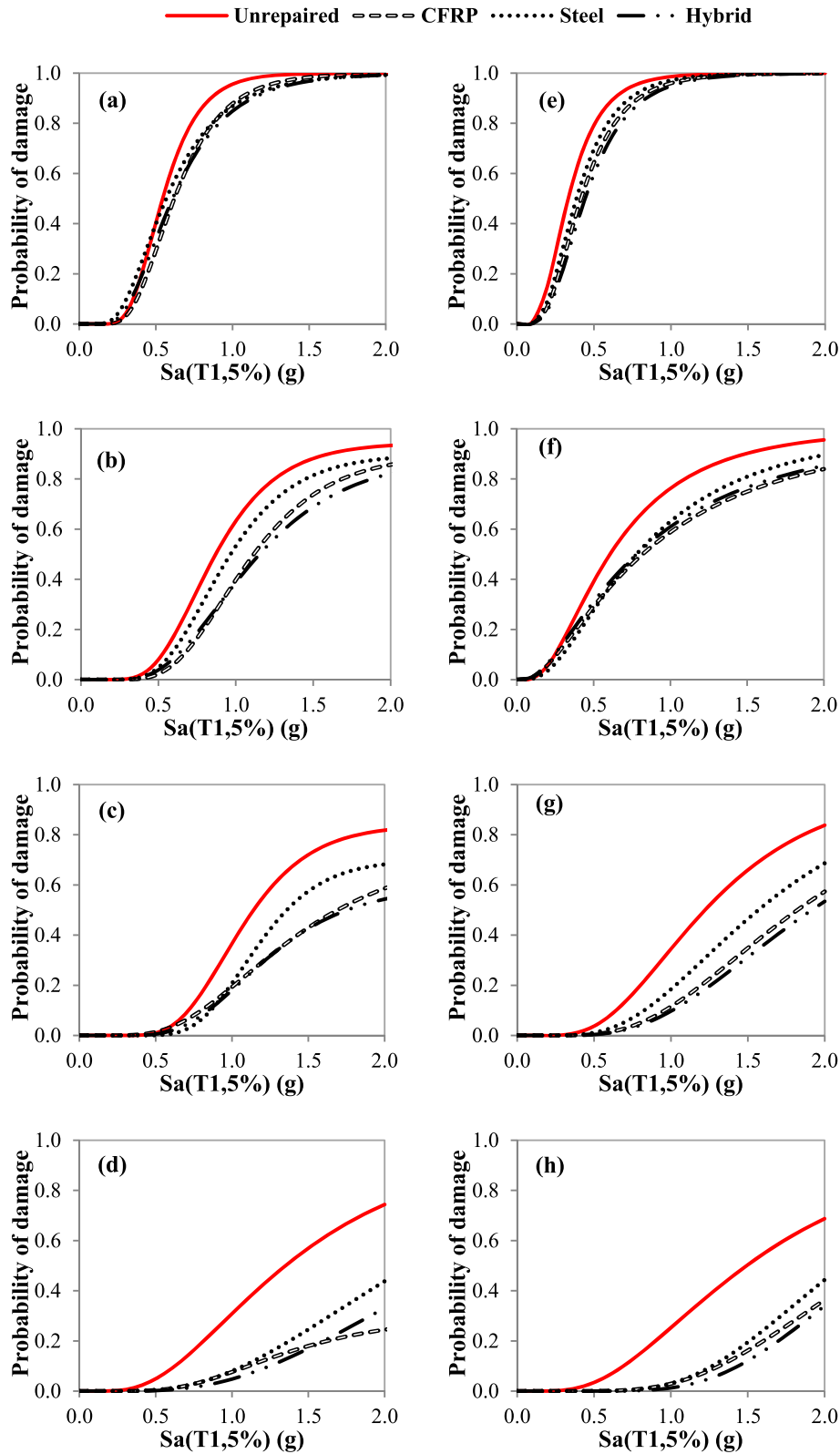
Fig. 13 Fragility curves for the unrepaired and repaired bridge under severe MS-severe AS sequence: ensemble 1 records **a** minor, **b** moderate, **c** extensive, and **d** collapse damage state; ensemble 2 records **e** minor, **f** moderate, **g** extensive, and **h** collapse damage state.

type (i.e., far-fault and near-fault) indicate the increase of difference (shift) between fragilities of the unrepaired and repaired bridge as the damage state progresses. While Fig. 13a, e (similarly, Fig. 14a, e) clearly indicate that the

fragility curves for the unrepaired bridge almost overlaps the repaired bridge under the minor damage state, the unrepaired bridge's vulnerability is significantly larger than the repaired bridge for the extensive and collapse damage states
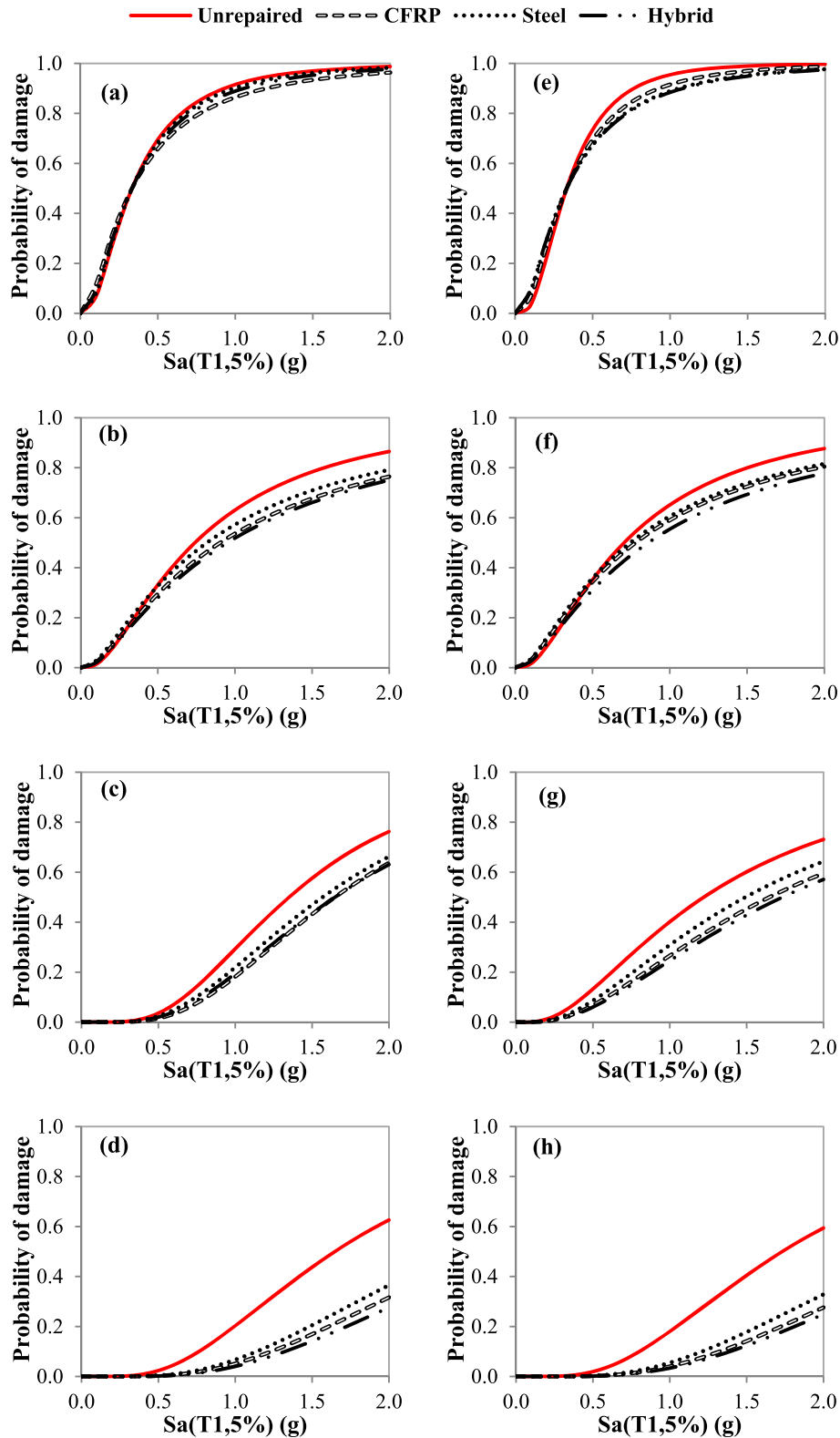
Fig. 14 Fragility curves for the unrepaired and repaired bridge under severe MS-moderate AS sequence: ensemble 1 records **a** minor, **b** moderate, **c** extensive, and **d** collapse damage state; ensemble 2 records **e** minor, **f** moderate, **g** extensive, and **h** collapse damage state.

(Figs. 13c, d, g, h, 14c, d, g, h). For instance, given the same probability of damage under the collapse damage state, the associated Sa of the unrepaired bridge is significantly less than that of the repaired bridge, irrespective of the repair jacket material. The fragilities accord to the obtained results from the IDA analyses results, where the repair jackets were more significant/critical for the severe MS-severe AS compared to the severe MS-moderate AS sequence. The

fragilities clearly indicate the importance of repair jackets as the damage state increases. However, the influence of different intensity MS-AS sequences is clear through comparison of Figs. 13 versus 14. The obtained fragilities demonstrate the decrease of vulnerability for the unrepaired and repaired bridge under severe MS-moderate AS compared to severe MS-severe AS. It also suggests that the fragilities of unrepaired and repaired bridge are shifted more toward right under severe MS-moderate AS compared to severe MS-severe AS, which signals the lesser significance of repair jackets under moderate AS.

The fragilities also reveal that the steel jacketed bridge exhibits the highest vulnerability compared to CFRP and hybrid repair jackets at all damage states under both earthquake types. The increased vulnerability of the steel jacketed bridge over the other two repair interventions is due to the increased seismic action attracted by the thick steel jacketed bridge pier (inertia force of the dynamic system is increased due to thick jacket). For the conventional thick steel jacketing, the column cross section (deadweight) is increased, which in turn absorbs larger seismic actions (Priestley et al. 1996). On the other hand, the CFRP and hybrid jackets demonstrated comparable fragilities under all damage states and earthquake types. Although the hybrid jacket showed marginal decreased vulnerability compared to the CFRP jacket. Although the conventional steel jacket was shown to be the most vulnerable repair alternative, however, the steel jacket exhibited larger hysteresis loops compared to the CFRP jacket. Thus, fragility function for different repair interventions should be considered along with further investigation to better select the appropriate repair alternative. The reduced service stiffness of earthquake damaged RC bridge piers is an issue which steel jackets may be more advantageous over CFRP jackets, as they could provide higher service stiffness for the repaired RC pier (Youm et al. 2006).

Moreover, the fragility functions provide additional valuable information in regards to far-fault and near-fault records effects under different damage states. The obtained fragilities indicate that the vulnerability under near-fault records is larger than far-fault records for the minor and moderate damage states under severe MS-severe AS sequence (e.g. Fig. 13b vs. f). However, for collapse damage state, the fragilities under far-fault ground motions were slightly higher than those of the near-fault records (e.g. Fig. 13d vs. h). The obtained results indicate higher vulnerability for far-fault AS under collapse damage state for severe MS-severe AS. For minor and moderate damage states the near-fault record aftershocks are more prominent over far-fault aftershocks. For severe MS-moderate AS the near-fault records were more prominent. The obtained results suggest that maybe there is a relation between significance of earthquake type (far-fault or near-fault) and intensity of the seismic sequence considered (severe MS-severe AS or severe MS-moderate AS) at different damage states which requires further studies. Needless to mention, this observation on earthquake type effect at various damage states is limited only to the present study, and may not be generalized.

8. Conclusions

Results from a comprehensive study on the seismic collapse capacity and seismic fragility of mainshock-damaged highway RC bridges—repaired with repair jackets—that are representatives of older bridge construction practice are presented in this paper. Analytical models of the studied bridge were subjected to numerous series of mainshock-aftershock sequences of various intensities of different fault-types (i.e., far-fault and near-fault). The seismic collapse capacity of mainshock-damaged bridge was investigated through an extensive number of IDA analyses. Three different repair techniques (CFRP, conventional thick steel and hybrid jacket) were considered. The collapse capacity and drift capacity of repaired bridge pier under severe MS-severe AS and severe MS-moderate AS were quantified. Different repair jackets were compared to address the differences that may arise on the post-repair response of rehabilitated bridges subjected to potential aftershocks. This study is limited to bridge with regular geometry under two ensembles of record sets in one direction. Additional studies considering irregular bridge configuration, near-fault mainshocks and far-fault aftershocks and vice versa, in addition to subduction, inslab and interface record sets and the inclusion of multi-directional loading should be conducted to further understand contributions of other parameters on the seismic response of bridges. The impact of jacket application incorporated in more complex numerical models considering soil-structure interaction, bearings at expansion joints (pounding and unseating), and abutment backfill soil effects, with the inclusion of pile-footing-pier failure would be contributory in this area. According to the obtained results the following conclusions can be drawn from the present study:

1. The existing damage under a severe MS attack may significantly jeopardize the post-MS resilience of substandard bridge piers. Damage accumulation and destabilizing moments due to geometric nonlinearities (P-Δ effect) are significant for the post-MS drift capacity of the single column bridge piers with lap-spliced reinforcement at column-footing interface.
2. Severe MS-severe AS sequences could significantly reduce the mean structural collapse capacity/maximum drift capacity of substandard bridge piers compared to severe MS only attacks. MS-AS seismic sequences incur numerous inelastic excursions, irrespective of the AS intensity (severe or moderate) or fault type (near-fault or far-fault).
3. Repair jackets contribute on the post-MS collapse capacity of damaged bridges subjected to aftershocks. Repair jackets application on damaged bridge piers are less effective for the severe MS-moderate AS sequence compared to severe MS-severe AS scenario. However, repair jackets are still essential for severe MS-moderate AS sequence.
4. Under minor and moderate damage states, near-fault aftershocks were prominent over far-fault aftershocks for severe MS-severe AS sequence. Under extensive

and collapse damages states far-fault aftershocks appeared more significant compared to near-fault aftershocks for severe MS-severe AS sequence. However, near-fault aftershocks were prominent at all damage states under severe MS-moderate AS.

5. The unrepaired and repaired bridge exhibit approximately identical fragilities under the minor damage state. The fragilities for the unrepaired and repaired bridge largely deviate from each other under the extensive and collapse damage states.
6. The conventional thick steel jacket exhibits the highest fragility compared to CFRP repair jacket.

Acknowledgments

Open Access

References

Abdelnaby, A., & Elnashai, A. (2014). Performance of degrading reinforced concrete frame systems under Tohoku and Christchurch earthquake sequences. *Journal of Earthquake Engineering 18*(7), 1009–1036. doi:10.1080/13632469.2014.923796.

Andrawes, B., Shin, M., & Wierschem, N. (2009). Active confinement of reinforced concrete bridge columns using shape memory alloys. *Journal of Bridge Engineering 15*(1), 81–89. doi:10.1061/ASCEBE.1943-5592.0000038.

Arias, A. (1970). A measure of earthquake intensity. In R. J. Hansen (Ed.), *Seismic design for nuclear power plants* (pp. 438–483). Cambridge, MA: MIT Press.

Aschheim, M., & Black, E. (1999). Effects of prior earthquake damage on response of simple stiffness-degrading structures. *Earthquake Spectra 15*(1), 1–24.

ATC-63. (2009). *Quantification of building seismic performance factors*. Redwood City, CA: FEMA P695.

Baker, J. W., & Cornell, C. A. (2006). *Vector-valued ground motion intensity measures for probabilistic seismic demand analysis*. Berkeley, CA: Pacific Earthquake Engineering Research Center, College of Engineering, University of California.

Baker, J. W., Lin, T., Shahi, S. K., & Jayaram, N. (2011). *New ground motion selection procedures and selection motions for the PEER transportation research program*. PEER report 2011/03, Berkeley, CA: Pacific Earthquake Engineering Research Center.

Bearman, C. F. (2012). *Post-earthquake assessment of reinforced concrete frames*. M.S. Thesis, Department of Civil and Environmental Engineering, University of Washington, Seattle, WA.

Berry, M. P., & Eberhard, M. O. (2007). *Performance modeling strategies for modern reinforced concrete bridge columns*. PEER report 2007/07. Berkeley, CA: Pacific Engineering Research Center, University of California.

Bianchi, F., Sousa, R., & Pinho, R. (2011). Blind prediction of a full-scale RC bridge column tested under dynamic conditions. In *Proceedings of the 3rd international conference on computational methods in structural dynamics and earthquake engineering* (*COMPDYN 2011*) *Corfu, Greece*, Paper no. 294.

Billah, A. M., Alam, M. S., & Bhuiyan, M. R. (2013). Fragility analysis of retrofitted multicolumn bridge bent subjected to near-fault and far-field ground motion. *Journal of Bridge Engineering*. doi:10.1061/(ASCE)BE.1943-5592.0000452.

Buckle, I., Friedland, I., Mander, J., Martin, G., Nutt, R., & Power, M. (2006). Seismic retrofitting manual for highway structures: Part 1-bridges (No. FHWA-HRT-06-032).

Calderone, A., Lehman, D. E., & Moehle, J. P. (2001). *Behavior of reinforced concrete bridge columns having varying aspect ratios and varying lengths of confinement*. Berkeley, CA: Pacific Earthquake Engineering Research Center.

California Department of Transportation. (2004). *Caltrans bridge design specification*. Sacramento, CA: California Department of Transportation.

Chang, L., Peng, F., Ouyang, Y., Elnashai, A. S., & Spencer, B. F, Jr. (2012). Bridge seismic retrofit program planning to maximize postearthquake transportation network capacity. *Journal of Infrastructure Systems 18*(2), 75–88.

Cho, J. Y., & Pincheira, J. A. (2006). Inelastic analysis of reinforced concrete columns with short lap splices subjected to reversed cyclic loads. *ACI Structural Journal 103*(2), 280–290.

Chopra, A. K., & Goel, R. K. (2002). A modal pushover analysis procedure for estimating seismic demands for buildings. *Earthquake Engineering and Structural Dynamics 31*(3), 561–582.

Cornell, C. A., Jalayer, F., Hamburger, R. O., & Foutch, D. A. (2002). Probabilistic basis for 2000 SAC federal emergency management agency steel moment frame guidelines. *Journal of Structural Engineering 128*(4), 526–533.

Di Sarno, L. (2013). Effects of multiple earthquakes on inelastic structural response. *Engineering Structures 56*, 673–681.

Dutta, A., & Mander, J. B. (1998). Seismic fragility analysis of highway bridges. In *Proceedings of the INCEDE-MCEER*

center-to-center project workshop on earthquake engineering Frontiers in transportation systems (pp. 22–23).

ElGawady, M., Endeshaw, M., McLean, D., & Sack, R. (2009). Retrofitting of rectangular columns with deficient lap splices. *Journal of Composites for Construction 14*(1), 22–35.

Fakharifar, M., Chen, G., Arezoumandi, M., & ElGawady, M. (2015a). Hybrid jacketing for rapid repair of seismically damaged reinforced concrete columns. *Transportation Research Record: Journal of the Transportation Research Board*. doi:10.3141/2522-07.

Fakharifar, M., Chen, G., Lin, Z., & Woolsey, Z. (2014a). Behavior and strength of passively confined concrete filled tubes. In *The 10th U.S. National conference on earthquake engineering: July 21–25, 2014, Anchorage, AL*.

Fakharifar, M., Chen, G., Sneed, L., & Dalvand, A. (2015b). Seismic performance of post-mainshock FRP/steel repaired RC bridge columns subjected to aftershocks. *Composites Part B: Engineering*. doi:10.1016/j.compositesb.2014.12.010.

Fakharifar, M., Dalvand, A., Arezoumandi, M., Sharbatdar, M. K., Chen, G., & Kheyroddin, A. (2014b). Mechanical properties of high performance fiber reinforced cementitious composites. *Construction and Building Materials 71*, 510–520. doi:10.1016/j.conbuildmat.2014.08.068.

Fakharifar, M., Dalvand, A., Sharbatdar, M. K., Chen, G., & Sneed, L. (2015c). Innovative hybrid reinforcement constituting conventional longitudinal steel and FRP stirrups for improved seismic strength and ductility of RC structures. *Frontiers of Structural and Civil Engineering*. doi:10.1007/s11709-015-0295-9.

Fakharifar, M., Sharbatdar, M. K., & Lin, Z. (2013). Seismic performance and global ductility of reinforced concrete frames with CFRP laminates retrofitted joints. In *Structures congress 2013* (pp. 2080–2093). ASCE.

Fakharifar, M., Sharbatdar, M. K., Lin, Z., Dalvand, A., Sivandi-Pour, A., & Chen, G. (2014c). Seismic performance and global ductility of RC frames rehabilitated with retrofitted joints by CFRP laminates. *Earthquake Engineering and Engineering Vibration, 13*(1), 59–73.

FEMA 356. (2000). *Prestandard and commentary for the seismic rehabilitation of buildings*. Prepared by ASCE for Federal Emergency Management Agency, Washington, D.C.

Ferracuti, B., Pinho, R., Savoia, M., & Francia, R. (2009). Verification of displacement-based adaptive pushover through multi-ground motion incremental dynamic analyses. *Engineering Structures 31*(8), 1789–1799.

Ferracuti, B., & Savoia, M. (2005). Cyclic behaviour of FRP-wrapped columns under axial and flexural loadings. In *Proceedings of the international conference on fracture, Turin, Italy*.

Filippou, F. C., Popov, E. P., & Bertero, V. V. (1983). *Effects of bond deterioration on hysteretic behaviour of reinforced concrete joints*. Report EERC 83-19. Berkeley, CA: Earthquake Engineering Research Center, University of California.

Fragiadakis, M., Pinho, R., & Antoniou, S. (2008). Modelling inelastic buckling of reinforcing bars under earthquake loading. In M. Papadrakakis, D. C. Charmpis, N.

D. Lagaros, Y. Tsompanakis, & A. A. Balkema (Eds.), *Progress in computational dynamics and earthquake engineering*. Leiden, Netherlands: Taylor & Francis.

Grelle, S. V., & Sneed, L. H. (2013). Review of anchorage systems for externally bonded FRP laminates. *International Journal of Concrete Structures and Materials 7*(1), 17–33. doi:10.1007/s40069-013-0029-0.

Harajli, M., Hamad, B., & Karam, K. (2002). Bond-slip response of reinforcing bars embedded in plain and fiber concrete. *Journal of Materials in Civil Engineering 14*(6), 503–511.

Haroun, M. A., & Elsanadedy, H. M. (2005). Fiber-reinforced plastic jackets for ductility enhancement of reinforced concrete bridge columns with poor lap-splice detailing. *Journal of Bridge Engineering 10*(6), 749–757.

Haselton, C. B., Liel, A. B., Taylor Lange, S., & Deierlein, G. G. (2008). *Beam-column element model calibrated for predicting flexural response leading to global collapse of RC frame buildings*. PEER report 2007/03. Berkeley, CA: Pacific Engineering Research Center, University of California.

HAZUS-MH. (2003). *Multi-hazard loss estimation methodology earthquake model*. HAZUS-MH MR3 technical manual. Washington, DC: Federal Emergency Management Agency (FEMA).

He, R., Sneed, L. H., & Belarbi, A. (2013). Rapid repair of severely damaged RC columns with different damage conditions: An experimental study. *International Journal of Concrete Structures and Materials 7*(1), 35–50. doi:10.1007/s40069-013-0030-7.

Huang, W., & Andrawes, B. (2014). Seismic performance of SMA retrofitted multiple-frame RC bridges subjected to stong mainshock-aftershock sequences. In *10th U.S. National conference on earthquake engineering (10NCEE) Anchorage, Alaska*.

Jirawattanasomkul, T. (2013). *Ultimate shear behavior and modeling of reinforced concrete members jacketed by fiber reinforced polymer and steel*. PhD thesis. Hokkaido University, Sapporo, Japan.

Kent, D. C., & Park, R. (1973). Cyclic load behaviour of reinforcing steel. *Strain 9*(3), 98–103.

Kunnath, S. K., El-Bahy, A., Taylor, A. W., & Stone, W. C. (1997). *Cumulative seismic damage of reinforced concrete bridge piers*. In Technical report NCEER (No. 97-0006). US National Center for Earthquake Engineering Research.

Lee, D. H., Kim, D., & Lee, K. (2009). Analytical approach for the earthquake performance evaluation of repaired/retrofitted RC bridge piers using time-dependent element. *Nonlinear Dynamics 56*(4), 463–482.

Lee, D. H., Park, J., Lee, K., & Kim, B. H. (2011). Nonlinear seismic assessment for the post-repair response of RC bridge piers. *Composites Part B Engineering 42*(5), 1318–1329.

Li, Y., Song, R., & Van De Lindt, J. W. (2014). Collapse fragility of steel structures subjected to earthquake mainshock-aftershock sequences. *Journal of Structural Engineering 140*(12), 04014095.

Li, Y., Song, R., van de Lindt, J., Nazari, N., & Luco, N. (2012). Assessment of wood and steel structures subjected to

earthquake mainshock-aftershock. In *15th world conference on earthquake engineering, Lisbon, Portugal*.

Lin, Z., Fakhairfar, M., Wu, C., Chen, G., Bevans, W., Gunasekaran, A. V. K., & Sedighsarvestani, S. (2013). *Design, construction and load testing of the Pat Daly Road Bridge in Washington County, MO, with internal glass fiber reinforced polymers reinforcement*. Report no. NUTC R275.

Mackie, K. R., & Stojadinovic, B. (2007). R-factor parameterized bridge damage fragility curves. *Journal of Bridge Engineering 12*(4), 500–510.

Madas, P., & Elnashai, A. S. (1992). A new passive confinement model for transient analysis of reinforced concrete structures. *Earthquake Engineering and Structural Dynamics 21*, 409–431.

Mander, J. B., Priestley, M. J. N., & Park, R. (1988). Theoretical stress–strain model for confined concrete. *Journal of Structural Engineering 114*(8), 1804–1826.

Marson, J., & Bruneau, M. (2004). Cyclic testing of concrete-filled circular steel bridge piers having encased fixed-based detail. *Journal of Bridge Engineering, ASCE 9*(1), 14–23.

Martinez-Rueda, J. E., & Elnashai, A. S. (1997). Confined concrete model under cyclic load. *Materials and Structures 30*(197), 139–147.

Menegotto, M., & Pinto, P. E. (1973). Method of analysis for cyclically loaded R.C. plane frames including changes in geometry and non-elastic behaviour of elements under combined normal force and bending. In *Symposium on the resistance and ultimate deformability of structures acted on by well defined repeated loads, international association for bridge and structural engineering, Zurich, Switzerland* (pp. 15–22).

Nazari, N., van de Lindt, J. W., & Li, Y. (2013). Effect of mainshock-aftershock sequences on woodframe building damage fragilities 1. *Journal of Performance of Constructed Facilities 29*(1), 04014036.

Nielson, B. G., & DesRoches, R. (2007). Analytical seismic fragility curves for typical bridges in the central and southeastern United States. *Earthquake Spectra 23*(3), 615–633.

PEER. (2010). Retrieved July 24, 2014, from http://nisee2.berkeley.edu/peer/prediction_contest/?page_id=25.

Pinto, A. V., Verzeletti, G., Pegon, P., Magonette, G., Negro, P., & Guedes, J., (1996). *Pseudo-dynamic testing of large-scale R/C Bridges*. Report EUR 16378, Ispra (VA), Italy.

Priestley, M. J. N., Calvi, G. M., & Kowalsky, M. J. (2007). *Displacement based seismic design of structures*. Pavia, Italy: Istituto Universitario di Studi Superiori Press.

Priestley, M. N., Seible, F., & Calvi, G. M. (1996). *Seismic design and retrofit of bridges*. New York, NY: Wiley.

Ribeiro, F. L., Barbosa, A. R., & Neves, L. C. (2014). Application of reliability-based robustness assessment of steel moment resisting frame structures under post-mainshock cascading events. *Journal of Structural Engineering 140*(8), A4014008.

Rodriguez, M. E., Botero, J. C., & Villia, J. (1999). Cyclic stress–strain behavior of reinforcing steel including effect of buckling. *Journal of Structural Engineering 125*(6), 605–612.

Saatcioglu, M., & Grira, M. (1999). Confinement of reinforced concrete columns with welded reinforced grids. *ACI Structural Journal 96*(1), 29–39.

Saatcioglu, M., & Yalcin, C. (2003). External prestressing concrete columns for improved seismic shear resistance. *Journal of Structural Engineering 129*(8), 1057–1070.

Schoettler, M. J., Restrepo, J. I., Guerrini, G., Duck, D. E., & Carrea, F. (2012). *A full-scale, single-column bridge bent tested by shake-table excitation*. Las Vegas, NV: Center for Civil Engineering Earthquake Research, Department of Civil Engineering, University of Nevada.

Scholz, C. H. (2002). *The mechanics of earthquakes and faulting*. Cambridge, MA: Cambridge University Press.

Scott, M. H., & Fenves, G. L. (2006). Plastic hinge integration methods for force-based beam–column elements. *Journal of Structural Engineering 132*(2), 244–252.

Seismosoft. (2013a). SeismoStruct—A computer program for static and dynamic nonlinear analysis of framed structures. www.seismosoft.com.

Seismosoft. (2013b). SeismoStruct ver. 6.0 and 7.0—Verification report.

Shamsabadi, A., Khalili-Tehrani, P., Stewart, J. P., & Taciroglu, E. (2009). Validated simulation models for lateral response of bridge abutments with typical backfills. *Journal of Bridge Engineering 15*(3), 302–311. doi:10.1061/(ASCE)BE.1943-5592.0000058.

Shinozuka, M., Feng, M. Q., Kim, H. K., & Kim, S. H. (2000). Nonlinear static procedure for fragility curve development. *Journal of Engineering Mechanics 126*(12), 1287–1295.

Sivaselvan, M., & Reinhorn, A. M. (1999). *Hysteretic models for cyclic behavior of deteriorating inelastic structures*. Report MCEER-99-0018, MCEER/SUNY/Buffalo.

Sivaselvan, M., & Reinhorn, A. M. (2001). Hysteretic models for deteriorating inelastic structures. *Journal of Engineering Mechanics ASCE 126*(6), 633–640, with discussion by Wang and Foliente and closure in Vol. 127, No. 11.

Spoelstra, M., & Monti, G. (1999). FRP-confined concrete model. *Journal of Composites for Construction, ASCE 3*, 143–150.

Tehrani, P., & Mitchell, D. (2013). Seismic risk assessment of four-span bridges in Montreal designed using the Canadian Bridge design code. *Journal of Bridge Engineering 19*(8), A4014002.

Terzic, V., & Stojadinovic, B. (2013). Hybrid simulation of bridge response to three-dimensional earthquake excitation followed by truck load. *Journal of Structural Engineering 140*(8), A4014010.

USGS. (2012). United States Geological Survey. http://www.usgs.gov/.

Vamvatsikos, D., & Cornell, C. A. (2002). Incremental dynamic analysis. *Earthquake Engineering and Structural Dynamics 31*(3), 491–514.

Villaverde, R. (2007). Methods to assess the seismic collapse capacity of building structures: State of the art. *Journal of Structural Engineering 133*(1), 57–66.

Vosooghi, A., & Saiidi, M. (2010). *Post-earthquake evaluation and emergency repair of damaged RC bridge columns using CFRP materials*. Rep. no. CCEER-10-05. Reno, NV:

Center for Civil Engineering Earthquake Research, Dept. of Civil Engineering, Univ. of Nevada.

Vosooghi, A., & Saiidi, M. S. (2012). Design guidelines for rapid repair of earthquake-damaged circular RC bridge columns using CFRP. *Journal of Bridge Engineering 18*(9), 827–836. doi:10.1061/(ASCE)BE.1943-5592.0000426.

White, T., & Ventura, C. E. (2004). Ground motion sensitivity of a Vancouver-style high rise. *Canadian Journal of Civil Engineering 31*, 292–307.

Xiao, Y., & Ma, R. (1997). Seismic retrofit of RC circular columns using prefabricated composite jacketing. *Journal of Structural Engineering 123*(10), 1357–1364.

Yang, J. (2009). *Nonlinear responses of high-rise buildings in giant subduction earthquakes*. PhD thesis. California Institute of Technology, CA, USA.

Yankelevsky, D. Z., & Reinhardt, H. W. (1989). Uniaxial behavior of concrete in cyclic tension. *Journal of Structural Engineering, ASCE 115*(1), 166–182.

Ying, X. F., Chen, G., Silva, P. F., LaBoube, R., & Yen, P. W. (2006). Thin steel sheet wrapping on RC columns and steel plate strengthening on beam-column joints for seismic ductility and capacity improvements. In *National conference on earthquake engineering, paper no. 513, conference proceeding, San Fransisco, CA, USA, April 18–22, 2006*.

Youm, K. S., Lee, H. E., & Choi, S. (2006). Seismic performance of repaired RC columns. *Magazine of Concrete Research 58*(5), 267–276.